UNIVERSITY OF HELSINKI REPORT SERIES IN PHYSICS

HU-P-D207

STRUCTURAL CHARACTERIZATION OF CELLULOSIC MATERIALS USING X-RAY AND NEUTRON SCATTERING

Paavo Penttilä

Division of Materials Physics
Department of Physics
Faculty of Science
University of Helsinki
Helsinki, Finland

ACADEMIC DISSERTATION

To be presented, with the permission of the Faculty of Science of the University of Helsinki, for public examination in Auditorium B123 of Exactum, Gustaf Hällströmin katu 2 B, on 1 November 2013 at 12 noon.

Helsinki 2013

Supervisor

Prof. Ritva Serimaa
Department of Physics
University of Helsinki
Helsinki, Finland

Pre-examiners

Prof. Markus B. Linder
Department of Biotechnology and Chemical Technology
Aalto University
Espoo, Finland

Assoc. Prof. Dorthe Posselt
Department of Science, Systems and Models
Roskilde University
Roskilde, Denmark

Opponent

Prof. Hans-Peter Fink
Fraunhofer Institute for Applied Polymer Research
Potsdam, Germany

Custos

Prof. Ritva Serimaa
Department of Physics
University of Helsinki
Helsinki, Finland

Report Series in Physics HU-P-D207
ISSN 0356-0961
ISBN 978-952-10-8934-3 (printed version)
ISBN 978-952-10-8935-0 (pdf version)
http://ethesis.helsinki.fi/
Helsinki University Print
Helsinki 2013

Do not concentrate too much on searching for something that you want to find.
Instead, open your eyes to see what your data wants to tell you.

Preface

This work has been carried out at the Department of Physics of the University of Helsinki and I would like to thank Prof. Juhani Keinonen for the opportunity to work there. In addition, I would like to acknowledge the other collaborating institutions, namely the Department of Food and Environmental Sciences and the Department of Chemistry of the University of Helsinki, VTT Technical Research Centre of Finland, Aalto University School of Science of Technology, Finnish Forest Research Institute (Metla), Åbo Akademi University, Innventia AB, Institut Laue-Langevin (ILL), and European Synchrotron Radiation Facility (ESRF). As for the financial side, I am truly thankful to the graduate schools Luonnonpolymeerien tutkijakoulu and BIOREGS, which enabled me to concentrate on science.

I owe a great debt of gratitude to my supervisor Prof. Ritva Serimaa, who believed in me and guided me gently throughout the whole work. She has always been encouraging and supportive of my ideas, yet in a reasonable way.

Besides my supervisor, I wish to thank all my co-authors and other collaborators for making this thesis possible. In particular, I would like to express my gratitude to Anikó for her hard work with the enzymes and for introducing me to new ways of thinking, and to Lasse for fruitful discussions and tasty beers. I also acknowledge Pirita and Petri for their important contributions to this work. I am thankful to Prof. Liisa Viikari, who was almost like a second supervisor to me and who, together with Prof. Maija Tenkanen, provided me with beautiful memories as well as invaluable contacts resulting from the numerous graduate school meetings and excursions. I would also like to thank Prof. Lennart Salmén for the possibility to visit his laboratory.

At the Department of Physics, I would like to thank the current and former staff members of the Laboratory of Electronic Structure, including Kirsi and Kari for introducing me to experimental science, Mika and Merja for helping me with all the instrumental issues, J-P, Inkeri, and Ville for sharing with me the moments of making great science, Juho and Patrik for otherwise good company, and, of course, Iina for preparing this job for me in the first place.

I sincerely thank all my friends (science and non-science) for being there during this journey and for giving me also other things to think about. My warmest thanks I owe to my family, including my parents and my sister, who provided me with everything that I required and supported my education and career at all times.

Helsinki, 3 September, 2013 *Paavo Penttilä*

P. Penttilä: Structural characterization of cellulosic materials using x-ray and neutron scattering, University of Helsinki, 2013, 59 pages + appendices. University of Helsinki, Report Series in Physics HU-P-D207.

Keywords: x-ray scattering, neutron scattering, cellulose, biomass nanostructure, biorefining

Classification (INSPEC): A6110F, A6112E, A6140K, A6146

Abstract

Cellulosic biomass can be used as a feedstock for sustainable production of biofuels and various other products. A complete utilization of the raw material requires understanding on its structural aspects and their role in the various processes. In this thesis, x-ray and neutron scattering methods were applied to study the structure of various cellulosic materials and how they are affected in different processes. The obtained results were reviewed in the context of a model for the cellulose nanostructure.

The dimensions of cellulose crystallites and the crystallinity were determined with wide-angle x-ray scattering (WAXS), whereas the nanoscale fibrillar structure of cellulose was characterized with small-angle x-ray and neutron scattering (SAXS and SANS). The properties determined with the small-angle scattering methods included specific surface areas and distances characteristic of the packing of cellulose microfibrils. Also other physical characterization methods, such as x-ray microtomography, infrared spectroscopy, and solid-state NMR were utilized in this work. In the analysis of the results, a comprehensive understanding of the structural changes throughout a range of length scales was aimed at.

Pretreatment of birch sawdust by pressurized hot water extraction was observed to increase the crystal width of cellulose, as determined with WAXS, even though the cellulose crystallinity was slightly decreased. A denser packing of microfibrils caused by the removal of hemicelluloses and lignin in the extraction was evidenced by SAXS. This resulted in the opening of new pores between the microfibril bundles and an increase of the specific surface area.

Enzymatic hydrolysis of microcrystalline cellulose (MCC) did not lead to differences in the average crystallinity or crystal size of the hydrolysis residues, which was explained to be caused by limitations due to the large size of the enzymes as compared to the pores inside the fibril aggregates. The SAXS intensities of rewetted samples suggested a modest opening of the fibrillar structure during hydrolysis, but no changes could be observed in the dry state.

Nanofibrillated cellulose (NFC) made of birch pulp with original and reduced xylan content was used as the substrate for enzymatic hydrolysis to reduce the effects of fib-

rillar aggregation. The results showed that the xylan present in the NFC with original xylan content limited the hydrolysis and caused an increase in cellulose crystallinity and crystal width, whereas the hydrolysis of NFC with reduced xylan content was more efficient and no increase in crystallinity or crystal size was detected. According to the SANS and SAXS results, the fibril network retained its shape in the NFC with original xylan content, whereas it gradually broke down during the hydrolysis in the NFC with reduced xylan content.

Cellulose whiskers were prepared from MCC without any major change in the cellulose crystallinity, as determined with WAXS and solid-state NMR. The drying behaviour of the whiskers was studied with SAXS by characterizing the structures formed under freeze-drying and under ambient conditions. The resulting structures were observed to be influenced by both the drying method and by surface charge neutralization.

List of papers

This thesis consists of an introductory part and five research articles, which are referred to by Roman numerals **I**–**V** throughout the text.

I **Penttilä, P. A.**, Kilpeläinen, P., Tolonen, L., Suuronen, J.-P., Sixta, H., Willför, S., and Serimaa, R. (2013). Effects of pressurized hot water extraction on the nanoscale structure of birch sawdust. *Cellulose*, DOI: 10.1007/s10570-013-0001-9

II **Penttilä, P. A.**, Várnai, A., Leppänen, K., Peura, M., Kallonen, A., Jääskeläinen, P., Lucenius, J., Ruokolainen, J., Siika-aho, M., Viikari, L., and Serimaa, R. (2010). Changes in submicrometer structure of enzymatically hydrolyzed microcrystalline cellulose. *Biomacromolecules*, 11:1111–1117.

III **Penttilä, P. A.**, Várnai, A., Pere, J., Tammelin, T., Salmén, L., Siika-aho, M., Viikari, L., and Serimaa, R. (2013). Xylan as limiting factor in enzymatic hydrolysis of nanocellulose. *Bioresource Technology*, 129:135–141.

IV **Penttilä, P. A.**, Várnai, A., Fernández, M., Kontro, I., Liljeström, V., Lindner, P., Siika-aho, M., Viikari, L., and Serimaa, R. (2013). Small-angle scattering study of structural changes in the microfibril network of nanocellulose during enzymatic hydrolysis. *Cellulose*, 20:1031–1040

V Rämänen, P., **Penttilä, P. A.**, Svedström, K., Maunu, S. L., and Serimaa, R. (2012). The effect of drying method on the properties and nanoscale structure of cellulose whiskers. *Cellulose*, 19:901–912.

Author's contribution

Paavo Penttilä (P. P.) planned and conducted most of the small- and wide-angle x-ray scattering (SAXS and WAXS) measurements in papers **II** and **V** and all of them in papers **I** and **III**. In paper **IV**, P. P. planned the neutron scattering measurements (SANS), participated in the experiment as the principal investigator, and was involved in the planning of the synchrotron SAXS measurements. Except for the determination of the crystal length in papers **II** and **V**, and the data normalization in paper **IV**, P. P. carried out the analysis of the scattering data in all of the papers. P. P. planned and conducted the static and dynamic FT-IR measurements in paper **III**. P. P. took the main responsibility for the evaluation and interpretation of the results and wrote most parts of papers **I**–**IV**. In paper **V**, P. P. actively participated in the interpretation of the results and the writing of the paper. Paper **II** has been previously included in the dissertation of Anikó Várnai (University of Helsinki, Department of Food and Environmental Sciences; VTT Science 17, Espoo 2012).

Other related work

List of publications which are relevant to this thesis but not included in it:

Testova, L., Nieminen, K., **Penttilä, P. A.**, Serimaa, R., Potthast, A., and Sixta, H. (2013). Cellulose degradation in alkaline media upon acidic pretreatment and stabilisation. *Carbohydrate Polymers*, DOI: 10.1016/j.carbpol.2013.01.093

Hauru, L. K. J., Ma, Y., Hummel, M., Alekhina, M., King, A. W. T., Kilpeläinen, I., **Penttilä, P. A.**, Serimaa, R., and Sixta, H. (2013). Enhancement of ionic liquid-aided fractionation of birchwood. Part 1: autohydrolysis pretreatment. *RSC Advances*, 3:16365–16373

Pahimanolis, N., Salminen, A., **Penttilä, P. A.**, Korhonen, J. T., Johansson, L.-S., Ruokolainen, J., Serimaa, R., and Seppälä, J. (2013). Nanofibrillated cellulose/carboxymethyl cellulose composite with improved wet strength *Cellulose*, 20:1459–1468.

Kontturi, E., Suchy, M., **Penttilä, P.**, Jean, B., Pirkkalainen, K., Torkkeli, H. M., and Serimaa, R. (2011). Amorphous Characteristics of an ultrathin cellulose film. *Biomacromolecules*, 12:770–777.

Tolonen, L. K., Zuckerstätter, G., **Penttilä, P. A.**, Milacher, W., Habicht, W., Serimaa, R., Kruse, A., and Sixta, H. (2011). Structural changes in microcrystalline cellulose in subcritical water treatment. *Biomacromolecules*, 12:2544–2551.

Penttilä, P. A., Suuronen, J-P., Kirjoranta, S., Peura, M., Jouppila, K., Tenkanen, M., and Serimaa, R. (2011). X-ray characterization of starch-based solid foams. *Journal of Materials Science*, 46:3470–3479.

Hirvikorpi, T., Vähä-nissi, M., Vartiainen, J., **Penttilä, P.**, Nikkola, J., Harlin, A., Serimaa, R., and Karppinen, M. (2011). Effect of heat-treatment on the performance of gas barrier layers applied by atomic layer deposition onto polymer-coated paperboard. *Journal of Applied Polymer Science*, 122:2221–2227.

Leppänen, K., Bjurhager, I., Peura, M., Kallonen, A., Suuronen, J-P., **Penttilä, P. A.**, Love, J., Fagerstedt, K., and Serimaa, R. (2011). X-ray scattering and microtomography study on the structural changes of never-dried silver birch, European aspen and hybrid aspen during drying. *Holzforschung*, 65:865–873.

Leppänen, K., Pirkkalainen, K., **Penttilä, P.**, Sievänen, J., Kotelnikova, N., and Serimaa, R. (2010). Small-angle x-ray scattering study on the structure of microcrystalline and nanofibrillated cellulose. *Journal of Physics: Conference Series*, 247:012030.

Contents

1 Introduction

1.1 Background

As a response to the limited availability of fossil fuels and a globally growing concern on the future of our environment, the demand for sustainable alternatives to oil and oil-based products is constantly increasing. Alternative resources to replace current raw materials are sought by the industry and, at the same time, sustainable materials are gaining more and more interest among consumers around the world. Potential raw materials to meet these challenges can be found in lignocellulosic biomass, which forms the feedstock for second generation biorefineries (Figure 1).

The principal component of biomass, cellulose, appears an intriguing raw material, being available worldwide with relatively low cost and, if acquired through socially sustainable routes, not competing with food production (Gomez et al., 2008; Graham-Rowe, 2011; Himmel et al., 2007). In addition to its traditional applications, such as construction materials or papermaking fibres, cellulose can be utilized in a vast amount of other ways, ranging from the use of the fibrils as part of composite materials (Faruk et al., 2012) to biofuels and other chemicals (Klemm et al., 2005; Ragauskas et al., 2006).

Despite a wide variety of current applications and uses of cellulosic materials, our knowledge of their fundamental structure is relatively limited (Chanzy, 2011; Chundawat et al., 2011; Klemm et al., 2005). Also the exact mechanisms underlying various treatments used to process lignocelluloses are not all well understood (Chundawat et al., 2011). In order to utilize the full potential of the available resources, to improve the current processes and to develop new ones, a better understanding on these mechanisms and their relation to the lignocellulose structure should be attained.

X-rays have been applied to shed light on the submicroscopic structure of cellulose and other biomaterials already for 100 years. The first cellulose diffraction pattern was published by a pair of Japanese doctoral students in 1913, only a year after the dis-

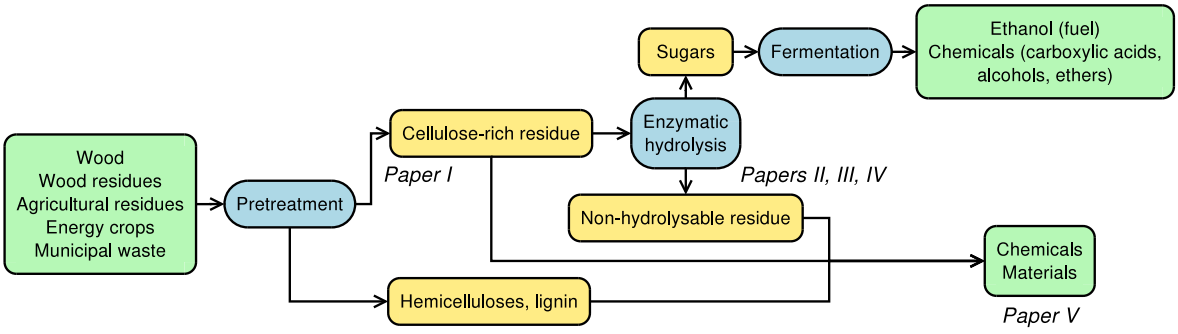

Figure 1. The concept of second generation biorefinery showing the relevancy of the papers included in this thesis. Adapted from Jørgensen et al. (2007).

covery of x-ray diffraction (Chanzy, 2011; Nishikawa and Ono, 1913). Later, with the development of more intensive laboratory sources and synchrotron radiation, the use of x-ray scattering in structural studies of cellulosic materials has become a standard. Even though several specialised scattering techniques for different purposes have been developed during the years, the most primary ones, wide and small-angle x-ray scattering, are still maintaining their status. In the meanwhile, these methods have been complemented by small-angle neutron scattering, which has shown notable benefits over x-rays in certain applications.

The development of new, sustainable cellulose-based products and materials in a larger scale can be aided by investigating the effects of the different processes on the biomass structure. An understanding on the fundamental level is also required for building a solid overall picture on the structural features of the materials and for being able to predict their behaviour under different conditions. In this thesis, x-ray and neutron scattering methods were applied to characterize the nanoscale structure of various cellulosic materials in order to extend our knowledge on the lignocellulose structure and to study the influences of various treatments to be performed in the context of second generation biorefinery.

1.2 Structure of wood-based biomass and its modification

The structure of native lignocellulosic biomass is highly hierarchical and complex, involving numerous components and different levels of organization. In order to understand the effects of the various structural modifications of cellulosic materials, a comprehensive and consistent picture of the original raw material should be adopted. This section takes an overview on the structure of cellulose and the composition of the wood cell wall, including an introduction to a few biomass processing methods relevant for this thesis.

1.2.1 Chemical composition

Cellulose

Wood-based biomass consists mainly of cellulose, hemicelluloses and lignin, which usually form over 95% of its total dry weight (Schultz and Taylor, 1989). The most abundant of these components, with a proportion of 40 to 45%, is cellulose, which is an unbranched homopolysaccharide consisting of β-D-glucopyranose molecules linked together by $(1 \rightarrow 4)$ glycosidic bonds (Figure 2a) (Schultz and Taylor, 1989; Sjöström, 1993). As each glucopyranose unit in the chain is oriented at an angle of 180° from the succeeding unit, the conformational repeating unit in a cellulose polymer is a cellobiose molecule, consisting of two glucopyranose units. The degree of polymerisation (DP) of native cellulose varies depending on its origin, but also due to the measurement technique used to obtain the molecular weight (Schultz and Taylor, 1989). Values

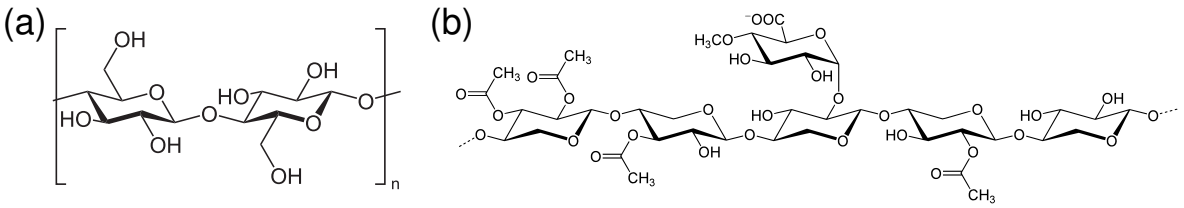

Figure 2. The chemical structure of (a) cellulose and (b) hardwood xylan.

around 10,000 have been obtained for wood cellulose and 15,000 for cotton cellulose, corresponding to a chain length of at least 5 µm in the fully extended state (Sjöström, 1993).

Hemicelluloses

Hemicelluloses are a group of heteropolysaccharides present in the plant cell wall. In wood they usually contribute to about 20 to 30% of the dry weight, but their composition and structure vary between wood species. Hemicelluloses generally consist of two or more different sugars, they can be branched, and they typically have a DP of 200 or below (Sjöström, 1993). The major hemicellulose in hardwoods, such as birch, is O-Acetyl-4-O-methylglucuronoxylan (Figure 2b), often simply called xylan. It has a backbone consisting of $(1 \rightarrow 4)$-linked β-D-xylopyranose units with occasional acetyl and uronic acid side groups, seven and one per ten xylose residues, respectively (Sjöström, 1993). In addition to xylan, which forms about 15 to 35% of the mass of dry hardwood, another typical hardwood hemicellulose is the unbranched glucomannan, contributing to 2 to 5% of the mass (Schultz and Taylor, 1989; Sjöström, 1993).

Lignin

Lignins are highly cross-linked polymers of phenylpropane units having various complicated structures. The lignin content of normal hardwood is typically between 20 and 25%, but its specific location as well as its composition and structure may vary significantly between different cell types and cell wall layers (Sjöström, 1993). The DP of lignin in hardwoods is below 20,000, even though it has a high polydispersity (Sjöström, 1993).

Other constituents and water

Besides cellulose, hemicelluloses and lignin, dry wood contains less than 5% of extraneous components, which do not contribute to its structural properties (Schultz and Taylor, 1989). These components include the so-called extractives, which are organic compounds like starch, pectins, simple sugars, aromatics and fatty acids. The extractives are soluble in selected neutral solvents and their composition is changed during wood storage (Sjöström, 1993). In addition to the extractives, wood contains typically less than 1% ash, which consists of inorganic compounds.

In a way, water may also be considered as a constituent of wood, because it has an important role in the structure of natural wood. Living trees contain up to 60% water, which can be roughly divided into two fractions based on its function and location (Schultz and Taylor, 1989). The fraction of water occupying the hollow centres of wood cells is called free water, whereas the water bound to the hydroxyl groups of cellulose and hemicellulose inside the cell wall is termed bound water. When dried under room temperature, the free water fraction is removed first and at least part of the bound water remains even after a long time. The swelling behaviour of wood and wood fibres, including the regions accessible to water, can be modified with chemical methods (Sjöström, 1993).

1.2.2 Cellulose in the plant cell wall

Structure of the plant cell wall

The plant cell wall consists of several layers, the thickest of which is the middle layer (S_2 layer) of the secondary wall (Sjöström, 1993). In higher plants like wood, this layer alone contributes to more than 50% of the cell wall thickness and contains most of their total cellulose. The inner structure of this cell wall layer consists of parallel fibrils of thickness in the order of 100 nm, which are helically circulating around the long axis of the cell (Figure 3). These fibrils consist of tight bundles of even thinner fibrils, where the smallest independent unit is called the cellulose microfibril (Donaldson, 2007). According to the generally accepted picture, plant-based cellulose microfibrils have cross-sections with a diameter varying roughly between 2 and 6 nm and containing essentially one cellulose crystallite, whereas their length extends to several hundred nanometres (Klemm et al., 2005; O'Sullivan, 1997).[1] In addition to crystalline cellulose, a significant fraction of cellulose exists in less ordered state, being referred to as amorphous cellulose. The location and nature of these two cellulose fractions varies between different parts of the cell wall (Ruel et al., 2012). The hierarchical composite structure is held together by a matrix formed by hemicelluloses and lignin.

Cellulose biosynthesis

Cellulose is known to be synthesized in the plasma membrane of the plant cell wall by enzymatic terminal complexes called rosettes (Brown Jr. and Saxena, 2000; Guerriero et al., 2010). One rosette consists of six subunits with hexagonal symmetry, thus having a total diameter of about 25 nm, and it is able to simultaneously synthesize 36 cellulose chains at maximum. The lateral dimensions of the resulting microfibril are partly determined by the geometry of the terminal complex, which can be observed for instance by comparing the microfibril cross-sections of algal celluloses synthesized by

[1] Varying terminology has been used for the elementary units of cellulose (Klemm et al., 2005; O'Sullivan, 1997), but here we adopt the definitions according to Brown Jr. and Saxena (2000) and Nishiyama (2009).

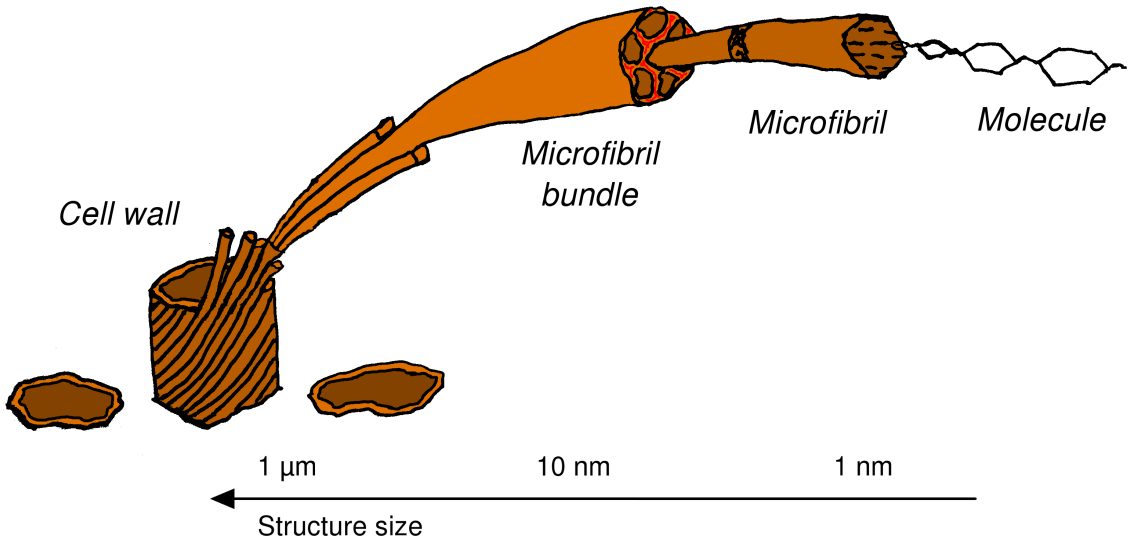

Figure 3. A sketch of the hierarchical structure of the wood cell wall.

differently shaped terminal complexes (Brown Jr. and Saxena, 2000; Guerriero et al., 2010; Moon et al., 2011). The eventual morphology of the microfibril, however, is not determined until the final aggregation and crystallization of the individually synthesized cellulose molecules and, at the moment, this particular step still remains to be elucidated (Guerriero et al., 2010). It has also been speculated that a complete microfibril bundle would be formed simultaneously by a group of rosettes (Guerriero et al., 2010), which might allow even more variation in the generated fibril morphology. Something that also remains to be explained in more detail, is how the different hemicelluloses are incorporated in the microfibril bundles (Awano et al., 2002).

Hemicelluloses and lignin in the plant cell wall

Hemicellulose content in the plant cell wall varies considerably between different cell types and different layers of the cell wall, as well as locally inside of these layers. In the middle layer of the secondary wall of hardwoods, the hemicellulose content is highest in the outer parts of the layer (Sjöström, 1993). The distribution of lignin varies also in the structure. About 20–25% of the total lignin is located in the intercellular spaces called middle lamella, whereas about 60–80% of it resides in the secondary cell wall (Schultz and Taylor, 1989; Sjöström, 1993). In some hardwoods, the lignin content of the secondary cell wall may be quite modest, even below 10% (Donaldson, 2007), but generally it is around 20–30% (Schultz and Taylor, 1989).

The detailed structure of the hemicellulose–lignin matrix surrounding the cellulose microfibrils and their bundles in the secondary plant cell wall is not well understood, even though attempts to describe the specific locations of the different cell wall components and their mutual interactions are constantly made (Olsson et al., 2011; Terashima et al., 2009). According to the current picture, mainly based on observa-

tions from the growing (primary) cell wall (Chundawat et al., 2011; Cosgrove, 2005; Gomez et al., 2008), the cellulose microfibrils or their bundles are surrounded by hemicelluloses, which maintain the rigid cellulose fibrils apart from each other and thereby increase the flexibility of the material. On the other hand, the hemicelluloses form also cross-links between the fibrils, which serves to anchor the fibrils to each other. The polysaccharides in the secondary plant cell wall, cellulose and hemicelluloses, are sealed by a lignin matrix (Chundawat et al., 2011; Gomez et al., 2008). The lignin acts as a waterproof mechanical reinforcement element, which is covalently linked to hemicelluloses and highly resistant to microbial digestion by enzymes. The locations and mutual interactions of the various constituents of biomass in relation to cellulose have also been discussed in papers **I** and **III** of this thesis.

1.2.3 Molecular und supramolecular structure of cellulose

Crystalline cellulose

Pure cellulose is known to crystallize in several allomorphs, although only two of them are found in nature (O'Sullivan, 1997; Zugenmaier, 2001). Cellulose Iα has a triclinic one-chain unit cell and cellulose Iβ a monoclinic two-chain unit cell, both of them containing parallel chains stacked in flat sheets on top of each other (Nishiyama et al., 2002; O'Sullivan, 1997). The Iβ allomorph (Figure 4) is known to be dominant in higher plants, but often they exist simultaneously (Atalla and VanderHart, 1984; O'Sullivan, 1997). The main difference between these two allomorphs is found in the stacking arrangement of the hydrogen-bonded sheets relative to each other, which could in principle allow them to be part of the same microfibril (Matthews et al., 2012). Other allomorphs, such as cellulose II or III_I, can be obtained by chemical and thermal treatments (O'Sullivan, 1997; Zugenmaier, 2001). In contrast to cellulose I, the chains forming the unit cell of cellulose II have antiparallel polarity (Kim et al., 2006; Langan et al., 2001).

In a cellulose Iβ crystal the cellulose chains are held together by several interactions (Gross and Chu, 2010; Nishiyama et al., 2002). Hydrogen bonds (O–H$\cdots$O) are formed between neighbouring residues of the same chain as well as between different chains in the same sheet, i.e. the plane determined by the glucose rings (perpendicular to the a axis in Figure 4). The stack of sheets is held together by weaker C–H$\cdots$O bonds, van der Waals interactions, and hydrophobic effects. According to computer simulations (Gross and Chu, 2010) the overall contribution of the intersheet interactions calculated per glucose unit is higher than that of the intrasheet O–H$\cdots$O hydrogen bonds.

Excluding the less ordered surface chains, each cellulose Iβ crystal in wood is thought to be formed of roughly 15 to 30 cellulose chains, thus having an agreement with the lateral widths of around 2 to 4 nm determined experimentally (Fernandes et al., 2011; Jakob et al., 1995; O'Sullivan, 1997). The shape of the microfibril cross-section varies between plant and wood species (Leppänen et al., 2009; O'Sullivan, 1997),

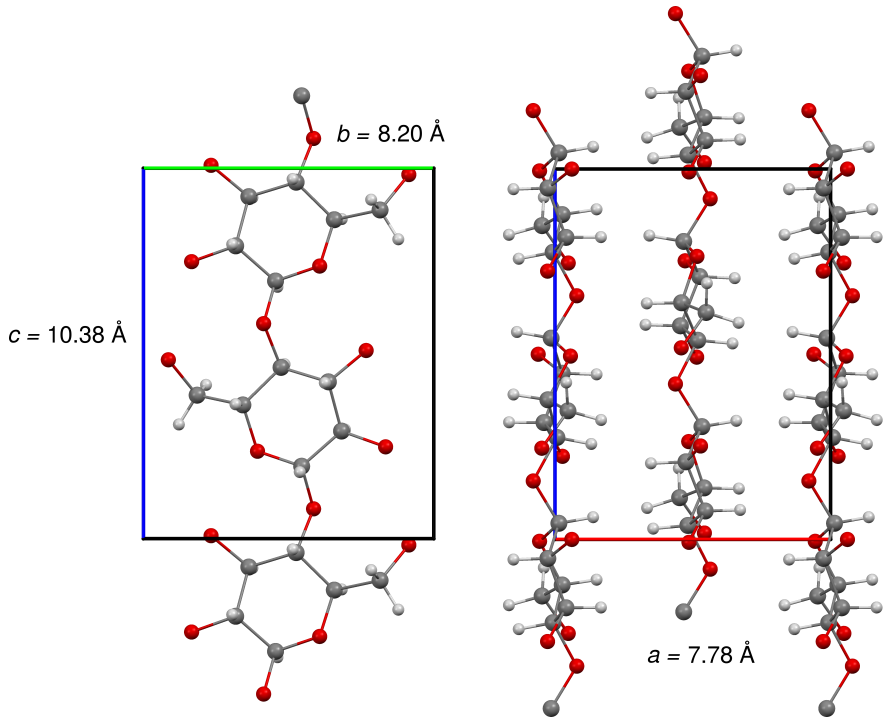

Figure 4. Unit cell of cellulose Iβ (Nishiyama et al., 2002) depicted along the a axis (left, centre chain only) and along the b axis (right).

even though no proper consensus on the topic seems to exist (Nishiyama, 2009). In the longitudinal direction of the chains, the crystalline order is maintained for a length of some tens of nanometres in wood, which has been deduced from the peak broadening observed in x-ray diffraction intensities (Andersson et al., 2003; Fernandes et al., 2011; Jakob et al., 1995; Leppänen et al., 2009). However, this crystal length value does not take into account any possible distribution of crystal lengths and, as illustrated by Astley and Donald (2001), it may emphasize larger crystal sizes. Whether the longitudinal disruption of the crystalline ordering after some tens of nanometres appears periodically, is therefore currently not known.

Amorphous cellulose

The division of cellulose into crystalline and amorphous fractions is more or less arbitrary and the exact form of non-crystalline cellulose and its subclasses are still under debate (Kondo et al., 2001; Kontturi et al., 2011; O'Sullivan, 1997). Usually, amorphous cellulose is referred to as cellulose lacking long-range order, which can be observed in x-ray diffraction patterns as an (isotropic) amorphous halo arising from the dimensions of the glucose units and corresponding to a distance of 0.4–0.5 nm (Paakkari et al., 1989). Sometimes the amorphous portion of cellulose is related to the conformationally disordered cellulose chains on crystallite surfaces (O'Sullivan, 1997), which can be distinguished with solid-sate NMR spectroscopy (Atalla and VanderHart, 1984; Evans

et al., 2005; Wickholm et al., 1998). In fact, collected experimental evidence currently suggests that most of the less ordered cellulose is located on the microfibril surfaces rather than within extensive amorphous regions along the microfibril (Driemeier and Bragatto, 2013; Fernandes et al., 2011; Nishiyama et al., 2003).

Regardless of its location, "amorphous" cellulose is seldom truly amorphous in the sense of a non-ordered, liquid-like isotropic distribution, because the molecules are believed to roughly share the same orientation with the crystals (O'Sullivan, 1997). Common orientation between the crystals and non-crystalline cellulose, as well as the matrix polymers, at least to some degree, has been shown experimentally with polarized Fourier-transform infra-red (FT-IR) spectroscopy (Olsson et al., 2011; Salmén et al., 2012; Stevanic and Salmén, 2009). Based on observations of FT-IR signals originating from various molecular groups, detected under different polarizations with respect to the longitudinal cell axis, it has been shown that both cellulose as well as the other components associated with it are aligned roughly in the same direction in wood. That is, the "amorphous" cellulose and the molecules of the "amorphous" hemicellulose matrix share a common preferred orientation with the cellulose crystallites in the cell wall. Moreover, physical interlinks between oriented hemicelluloses and cellulose have been demonstrated (Åkerholm and Salmén, 2001) and it has been proposed that the less ordered parts of the cellulose microfibrils, i.e. probably the cellulose chains at the crystallite surfaces, are located closer to lignin, hemicelluloses, and water (Fernandes et al., 2011) and that they would serve to complement the amorphous hemicellulose (Driemeier and Bragatto, 2013). In paper **III** of this thesis, a preferred orientation of a fraction of xylan with respect to cellulose was observed with dynamic FT-IR spectroscopy in birch-based nanofibrillated cellulose and the interactions between the different components were discussed.

Fibrillar structure of cellulose

The basic cohesive unit in wood samples seems to be the aggregate or bundle of cellulose microfibrils, which can be observed in microscopy images (Donaldson, 2007; Fahlén and Salmén, 2003; Fink et al., 1990; Frey-Wyssling, 1954; O'Sullivan, 1997). Even though the bundles (sometimes called macrofibrils) are directly observable with microscopic techniques, their inner structure is not completely understood and various models have been proposed for it (Driemeier and Bragatto, 2013; Fahlén and Salmén, 2005; O'Sullivan, 1997). Based on current experimental evidence, a cross-sectional model sketched in Figure 5 is proposed and will be discussed in the following.

In the fibrillar model presented in Figure 5, the microfibrils, consisting of about 36 parallel cellulose chains in a crystal, are arranged into bundles with outer lateral dimensions in the order of 20 nm (Donaldson, 2007; Fahlén and Salmén, 2003; Klemm et al., 2005; O'Sullivan, 1997). The spaces between the microfibrils are occupied by amorphous cellulose and by some hemicelluloses, being at least partly accessible to

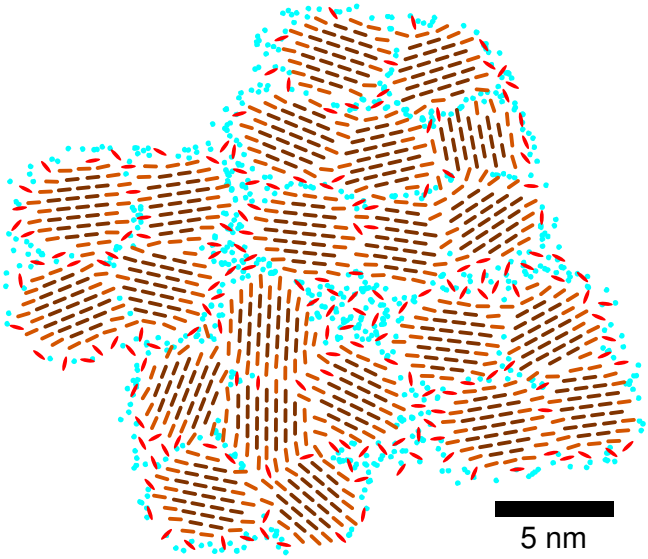

Figure 5. A schematic drawing of cellulose microfibril bundles in the secondary cell wall of wood. The dark brown lines correspond to the projections of crystalline cellulose molecules and the lighter brown lines to less ordered cellulose. Hemicelluloses are depicted in red and hydrated parts in blue. Lignin has been omitted for simplicity.

water (Driemeier and Bragatto, 2013; Fernandes et al., 2011). The microfibril bundles are surrounded by hemicelluloses and lignin, also partly accessible for water. Among the microfibril aggregates, elongated water-filled pores exist, which are caused by the imperfect packing of the microfibrils and bundles of them (Driemeier and Bragatto, 2013; Fahlén and Salmén, 2005).

The orientation and directionality of the cellulose microfibrils or crystals in the bundles are important factors related to the ultrastructure and reactivity of cellulose. The microfibrils of each bundle share a common directionality in their longitudinal axis, but the equatorial orientation of the crystals around this axis may possibly vary (Driemeier and Bragatto, 2013), as is the case at least for the bundles (Lichtenegger et al., 1999; Nishiyama, 2009). The varying orientation of the crystallites inside a microfibril bundle opens the speculation for the role of amorphous cellulose as a less ordered transition zone between the adjacent crystals (lighter brown chains in Figure 5) (Driemeier and Bragatto, 2013), which could partly explain the necessity of amorphous cellulose in all kinds of cellulosic substances with native microfibrils present. The directionality of the longitudinal axis, i.e. polarity, of adjacent microfibril bundles, on the other hand, varies randomly, enabling the intermingling of chains of different polarity during mercerization and formation of the cellulose II allomorph (Kim et al., 2006; O'Sullivan, 1997). The opposite polarity might also serve to induce disorder on the bundle surface.

The internal structure of cellulose microfibrils in the longitudinal direction deserves also attention. Even though the line broadening in x-ray diffraction experiments shows

that the long-range order in the cellulose crystals in this direction extends only to some tens of nanometres, other experimental evidence gained by small-angle neutron scattering of deuterated ramie fibres suggests that there are localized regions of disorder present with much longer, yet regular, spacing (Nishiyama et al., 2003). These regions could be originally caused by a disturbance in the function of the terminal complex during the biosynthesis of the microfibril. As an interesting detail pointed out by Fernandes et al. (2011), the interval of the disordered regions roughly corresponds to the average distance between chain ends in a 24-chain microfibril, namely 200 nm, if equally long chains with a random distribution of chain ends are assumed. Another potential cause for the defects could be some internal strains in the microfibril (Nishiyama, 2009; Nishiyama et al., 2003). Even though their origin remains under debate, the distance between the disordered regions corresponds well to the levelling-off DP of acid hydrolysis and the length of the residual cellulose particles, which suggests that these small disordered regions, covering only a few glucose units at a separation of about 300 units, would correspond to the fraction of cellulose most easily removed by acid hydrolysis (Nishiyama et al., 2003). In this context, it seems logical that the disruption of the long-range order in the crystallites at shorter and possibly irregular intervals would be caused by twisting, bending, or some other less dramatic crystal defects, possibly confined inside the crystalline core of the microfibril, rather than by an extensive discontinuity in the crystallite and microfibril. Twisting of cellulose microfibrils has been observed with microscopic techniques for instance in tunicin-based and algal celluloses (Elazzouzi-Hafraoui et al., 2008; Hanley et al., 1997) and predicted by computer simulations of cellulose Iβ crystals (Matthews et al., 2006; Paavilainen et al., 2011)

1.2.4 Processed biomass and cellulose

The utilization of ligno-cellulosic biomass in the context of biorefining requires various treatments and modifications to be carried out in order to obtain the final products (Figure 1). The main route followed by the works included in this thesis is that aiming at the production of bioethanol and other chemicals from depolymerised biomass polysaccharides. First, the biomass is subjected to a pretreatment (paper **I**), which serves to remove some of the non-cellulosic components and to prepare the material for the following steps. After the pretreatment, the residual polysaccharides are enzymatically hydrolysed to soluble sugars (papers **II**–**IV**), which can be fermented to ethanol and other chemicals (Chundawat et al., 2011; Gomez et al., 2008; Jørgensen et al., 2007). Currently, the conversion of cellulosic biomass to fermentable sugars represents the major bottleneck reducing the cost-effectiveness of the process (Viikari et al., 2012).

The depolymerisation of the cellulose in a second generation biorefinery is catalysed by enzymes, which represent a milder and more controllable option as compared for in-

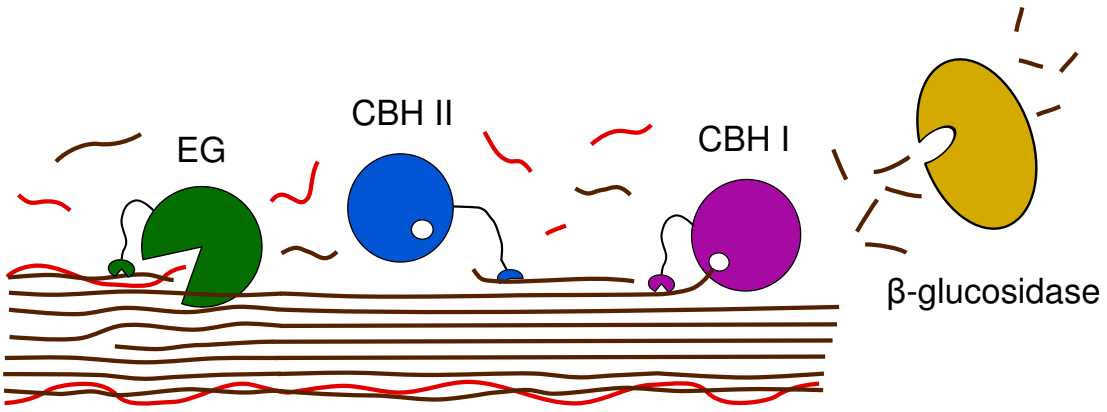

Figure 6. The enzymes typically involved in the hydrolysis of cellulose: cellobiohydrolase I (CBH I) and II (CBH II) hydrolyse the cellulose chains processively from their reducing and non-reducing ends, respectively, whereas the endoglucanases (EG) cut the chains at random. The cellobiose units produced by the CBHs are degraded to glucose by β-glucosidase. Cellulose chains are depicted as brown lines and hemicellulose in red. Original idea of figure by Teeri (1997).

stance to acid hydrolysis (Chundawat et al., 2011; Hu and Ragauskas, 2012). However, despite that the hydrolysis involves distinct types of enzymes working in synergy with each other (Figure 6), the naturally complex multi-component structure of biomass creates serious challenges for the deconstruction, in which the term "biomass recalcitrance" is often used to describe this natural resistance (Himmel et al., 2007; Mosier et al., 2005). Probably the single most significant limiting factor for the enzymatic hydrolysis of natural biomass is the physical barrier formed by the hemicellulose–lignin matrix, but also other factors related to the structure and morphology have been discussed in the literature (Alvira et al., 2010; Chundawat et al., 2011; Mansfield et al., 1999; Mosier et al., 2005). Overcoming these various limitations, including microfibrillar aggregation and hemicellulose content, was the motivation for papers **II**–**IV** of this thesis, which investigated the structural changes introduced by the enzymes in cellulosic substrate materials.

The natural recalcitrance of cellulosic biomass towards enzymatic hydrolysis can be reduced by pretreatments, which increase the accessibility of the enzymes to their cellulosic substrates (Alvira et al., 2010; Chundawat et al., 2011). This can be achieved by the removal or modification of the hemicellulose–lignin matrix, which directly protects the cellulose against microbial attack, as well as by loosening the tight packing of native cellulose fibrils. In an ideal case, the matrix components can be extracted in a controlled manner, which enables their utilization in other applications. An alternative, or often accompanying, mechanism for a pretreatment is to modify the crystalline structure of cellulose, either by decreasing the crystallinity or by inducing a transformation from the native cellulose I allomorph to a less resistant one. The choice of the applied pretreatment method depends on the targets of the pretreatment as well as on

the properties of the particular raw material.

The pretreatment of lignocellulosic biomass for enzymatic hydrolysis can be realized using water-based systems, where factors including the temperature, pH, and treatment duration, collectively described by so-called severity factors, affect the resulting structure (Pedersen and Meyer, 2010). One of the most prominent pretreatment methods in this field is pressurized hot water extraction, in which the hemicelluloses and a part of lignin are dissolved by liquid water at elevated temperatures and the structure is modified to be better accessible to the enzymes (Alvira et al., 2010; Mosier et al., 2005). The treatment can be carried out using either a flow-through or a batch system and the temperature of the water is typically kept between 160 and 240°C. The benefits of this pretreatment method as compared to many others are related to its neutral conditions and lack of required other chemicals, whereas its downsides include high water input and high energy consumption. The effects of pressurized hot water extraction on the nanoscale structure of birch sawdust were the subject of paper **I** of this thesis. A more recently evolved alternative for water-based pretreatment systems are ionic liquids, which dissolve the cellulose and other components and lead to a modification of the cellulose crystal structure to a more readily hydrolysable form (Cheng et al., 2011; Kilpeläinen et al., 2007; Samayam et al., 2011).

Apart from the processing methods of wood-based biomass directly related to biorefining, several others are also relevant for this thesis. One of these processes is pulping, which forms the basis of modern industrial papermaking. In kraft pulping, the dominant method of chemical pulping, cellulose fibres are separated from wood by pressurized alkaline cooking at elevated temperatures (Sjöström, 1993). The treatment removes such a large proportion of lignin that the fibres are easily liberated, but at the same time also the polysaccharides are at least partly degraded. Both cellulose and hemicelluloses are degraded by peeling from their chain ends and the structure of xylan is altered by the cleavage of acetyl groups (Sjöström, 1993). The residual lignin remaining after the pulping process may be removed by bleaching, which also serves to improve the overall cleanliness of the pulp (Sjöström, 1993). As the pulping removes most of the matrix materials from between the cellulose microfibrils, irreversible cross-linking of microfibrils and their bundles may take place when the pulp is dried (Pönni et al., 2012). This effect has been termed microfibril coalescence (Pönni et al., 2012) and it might at least partly explain the detected increase in the lateral crystal size of cellulose during pulping (Leppänen et al., 2009). A possibly similar effect has been discussed in relation to pressurized hot water extraction in paper **I** of this thesis.

Wood pulp can be further refined to obtain other materials. For instance mechanical homogenization of wood pulp can be used to obtain fibrillated cellulose (Herrick et al., 1983; Turbak et al., 1983), where the cellulose fibrils can be separated from each other even down to the level of individual microfibrils (Arola et al., 2013; Pääkkö et al., 2007; Siró and Plackett, 2010). The network of fibrils formed in this process has a

high capacity for water uptake and its crystallinity has been slightly decreased. These micro- and nanofibrillated cellulose (MFC and NFC) materials have several potential applications as such or as part of composite materials (Faruk et al., 2012; Moon et al., 2011). In this thesis, however, NFC was used as a model system in order to investigate the action of cellulose hydrolysing enzymes on the structure of the cellulose fibrils and the fibril network (papers **III** and **IV**).

More robust modifications to cellulosic substances may be introduced by acid hydrolysis. The typical hardwood hemicelluloses, xylan and glucomannan, are hydrolysed to monosaccharides already by dilute acids (Sjöström, 1993), but cellulose, especially crystalline cellulose, is more resistant to acidic cleavage. When hydrolysed with acids, cellulose shows a so-called levelling-off DP, which is reached already at the early stages of the hydrolysis (below 10% degree of hydrolysis) (Battista, 1950; Nishiyama et al., 2003). As mentioned in Section 1.2.3, a correspondence between the levelling-off DP and the distance between the periodic amorphous regions first attacked by the hydrolysis has been found in ramie cellulose microfibrils (Nishiyama et al., 2003). Acidic hydrolysis of wood fibres can be used to prepare microcrystalline cellulose (MCC), which after neutralization and spray-drying consists of porous micrometre scale particles formed by aggregated residual microfibril bundles (Moon et al., 2011) and has a cellulose DP of 150 to 300 (Klemm et al., 2005). Further hydrolysis of MCC produces cellulose nanocrystals (CNC) or cellulose whiskers, which are highly crystalline, rod-like nanoparticles 3–30 nm in width and tens to hundreds of nanometres in length (Azizi Samir et al., 2005; Dong et al., 1998; Eichhorn, 2011; Moon et al., 2011; Rånby, 1951). If sulphuric acid is used for the hydrolysis, the surface of the particles becomes negatively charged due to the presence of sulphate groups. In this thesis, the drying behaviour of cellulose whiskers prepared by sulphuric acid hydrolysis from different MCCs was studied in paper **V**, whereby also the influence of surface charge neutralization was examined. In paper **II** the effects of enzymatic hydrolysis on the structure of MCC were investigated.

What links together all the processing methods discussed above, is that in all of them the structure of cellulose and cellulose microfibrils is modified only partially. The native fibrillar structure consisting of microfibrils associated together to form larger bundle structures is retained. In this thesis, the focus is in the effects of various treatments on these structures, that is, the structures on the level of cellulose crystals and above.

1.3 Structural characterization of cellulosic materials

This section aims at presenting an introduction to a few experimental techniques used to characterize the nanoscale structure of cellulosic materials. As the main focus of this thesis is in the application of scattering methods, x-ray scattering in particular, the discussion will be biased in that direction.

1.3.1 Cellulose crystallinity

Similar to many other semicrystalline polymers, the radially averaged wide-angle x-ray scattering (WAXS) pattern of cellulose consists of a smooth amorphous intensity distribution topped by peaks arising from crystals of dimensions in the nanometre scale. In principle, the powder diffraction pattern of a semicrystalline polymer sample can be used to determine its crystallinity, defined as the dry mass fraction of the sample in crystalline state (Gedde, 1995). This is based on the principle that the total coherent scattering from all electrons in the sample is independent of the state of aggregation of their host atoms (Gedde, 1995). However, as it comes to cellulose, various challenges are faced by attempts to experimentally determine the crystallinity of real samples. One of the most fundamental challenges is related already to the definition of crystallinity. As pointed out by Driemeier and Calligaris (2011), the definition of a crystal given by the International Union of Crystallography is based on the existence of relatively sharp Bragg peaks detected by an x-ray diffraction experiment. However, because of the small crystallite dimensions, the diffractogram of cellulose typically contains rather broad peaks (Figure 7), which are, apart from a few exceptions, not distinguishable from each other. In addition to raising a contradiction with the definition of crystallinity, the overlapping of broad peaks seriously complicates the accurate determination of cellulose crystallinity from WAXS patterns (Driemeier and Calligaris, 2011). In order to avoid the terminological contradiction in practice, terms like “crystallinity index” or “apparent crystallinity” are sometimes favoured over the term “(degree of) crystallinity” in the literature.

Another challenge for the determination of crystallinity of cellulose is related to the general composition of cellulosic samples. This is because the assumption of a simple two-phase system with separate crystalline and amorphous fractions is not valid in most cases (Driemeier and Bragatto, 2013; Nishiyama et al., 2012). As already discussed in Section 1.2.3, various degrees of order exist within the amorphous fraction. Moreover, the additional components present in many cellulosic materials, mainly hemicelluloses and lignin, are for the sake of simplicity approximated to belong to the amorphous phase. As no larger crystals are formed by the branched hemicelluloses, this assumption can be held as justified. However, it has been suggested that some well-ordered hemicelluloses on the cellulose crystal surface may contribute to the lateral crystal size determined from peak broadening in WAXS (Driemeier et al., 2011), in which case they

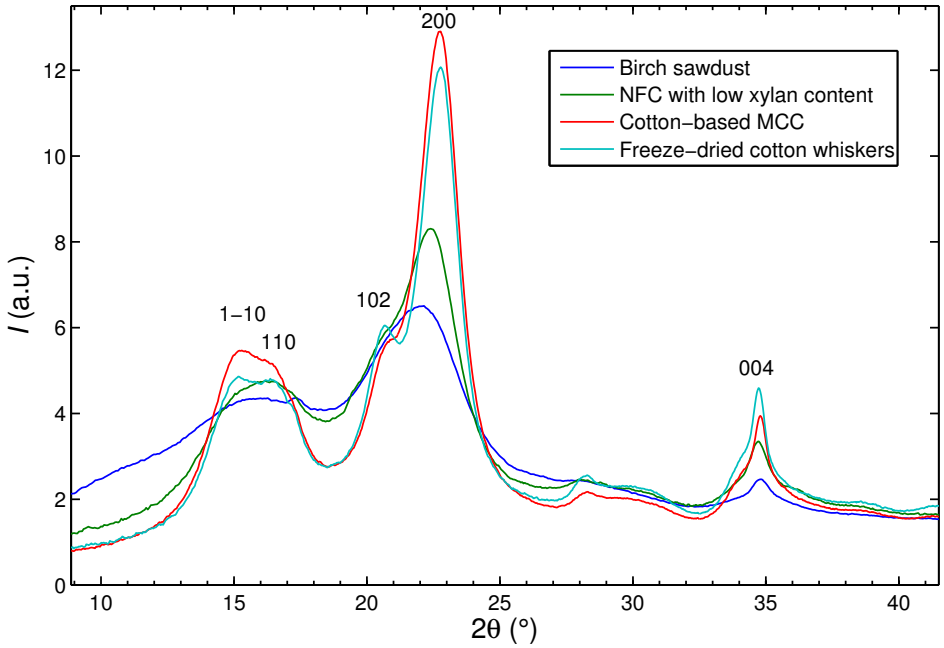

Figure 7. Wide-angle x-ray scattering (WAXS) intensities of various cellulosic samples showing the main reflections of cellulose Iβ (Nishiyama et al., 2002). The data has been taken from the papers and the results for crystallinity and crystal size are shown in Table 1.

would also affect the crystallinity determination with methods based on peak fitting.

Furthermore, the definition of crystallinity based on x-ray diffraction deviates from the concept of crystallinity encountered in relation to spectroscopic techniques, such as solid-state ^{13}C cross-polarization/magic-angle spinning nuclear magnetic resonance (CP/MAS NMR) spectroscopy, Fourier-transform infrared (FT-IR) spectroscopy, or FT Raman spectroscopy (Evans et al., 2005; Park et al., 2010; Schenzel et al., 2005; Wickholm et al., 1998). As these methods are based on the detection of signals from molecular groups separated in space, they are sensitive to short-range order and independent of any long-range periodicity. In particular for solid-state NMR, different signals have been indexed to cellulose chains inside the crystal and on its surface (Atalla and VanderHart, 1984; Evans et al., 2005; Wickholm et al., 1998). Moreover, the signals from molecular groups near crystal surfaces have been divided based on different degrees of order and accessibility of the surfaces (Wickholm et al., 1998). When comparing between crystallinity values obtained with different methods, care should be taken also regarding the terminology. As an example, the term "paracrystalline cellulose" appears in relation to NMR spectroscopy meaning both an intermediate form of structure between crystalline cellulose and disordered surface chains (Wickholm et al., 1998) and the less ordered surface chains in general (Ioelovich et al., 2010). In the field of x-ray diffraction, paracrystallinity refers to the fluctuations of the unit cell

dimensions within a crystallite (Hosemann and Bagchi, 1962).

In addition to deviations between different experimental techniques, the numerical value of the crystallinity also depends on the method used to obtain it from the experimental data. Different methods to extract the cellulose crystallinity from WAXS data have been reviewed and compared elsewhere (Bansal et al., 2010; Park et al., 2010; Thygesen et al., 2005), but a few of them are discussed here. The most commonly applied method is the peak-height method presented by Segal et al. (1959) (also known as the Segal method), which is based on the comparison of intensity values at only two points of the intensity profile and mainly used for its simplicity. Despite being able to highlight crystallinity differences among samples of the similar kind, which may correlate with crystallinities determined with other methods, the peak-height method is known to yield systematically higher values than most of the other methods and cannot be used to determine the absolute crystallinity of a cellulosic sample (Bansal et al., 2010; Park et al., 2010; Thygesen et al., 2005). In addition, because the calculation of the crystallinity with this method does not take into account the peak shape, the values are significantly affected by the crystal size and shape.

The more reliable methods for cellulose crystallinity determination from WAXS data rely on the utilization of the whole x-ray diffractogram (Bansal et al., 2010; Park et al., 2010; Thygesen et al., 2005). In that, the most difficult task is the separation of the crystalline and amorphous components of the scattering intensity. This can be done in practice by using a smooth curve to connect the tails of well-resolved diffraction peaks, as in the original Ruland–Vonk method (Ruland, 1961; Vonk, 1973), or by approximating the amorphous background by a function below the contribution of the diffraction peaks, as in Rietveld refinement (Thygesen et al., 2005). Alternatively, the amorphous background can be determined experimentally by measuring the scattering of an amorphous standard (Andersson et al., 2003; Thygesen et al., 2005). In many cases, however, problems arise due to the lack of a universal amorphous background (Driemeier and Calligaris, 2011; Thygesen et al., 2005). To account for these obscurities, a new and highly sophisticated, yet slightly complicated, method was presented by Driemeier and Calligaris (2011). This method is based on Rietveld modelling, which basically contains a least-squares fit to the intensity by a number of Bragg peaks, and takes into account the effects of preferred orientation, incoherent scattering, moisture content, and compositional deviations. However, some of the values obtained with this method may be overestimated, which could be due to effects caused by the choice of a Lorentzian peak profile (Driemeier et al., 2011).

In the light of the above discussion, it is not surprising that the crystallinity values reported in the literature even for similar cellulosic samples contain considerable variation. If the less reliable methods used to determine the crystallinity from WAXS intensities are excluded, crystallinity values of 40–70% for MCC are most often encountered in the literature (Bansal et al., 2010; Leppänen et al., 2009; Park et al., 2010;

Thygesen et al., 2005), whereas those for pulp and wood are somewhat lower, at about 30–55% (Andersson et al., 2003; Leppänen et al., 2009; Thygesen et al., 2005). Here it should be noted that in some cases the sample crystallinity may deviate significantly from the cellulose crystallinity, because of a large amount of other (non-crystalline) components present in the sample. Due to this fact, the cellulose crystallinity of most wood-based cellulose I samples seems to be roughly in the range from 40 to 70%, independent of their origin (Andersson et al., 2003; Thygesen et al., 2005). Compared to these values and taking their variation into account, the crystallinities determined by solid-state NMR are often in the same range and show correlations with x-ray crystallinities (Andersson et al., 2003; Park et al., 2010; Thygesen et al., 2005; Tolonen et al., 2011). In relation to this thesis, the crystallinity of cellulose was studied with WAXS in papers **I**–**III** and **V**. In paper **V** the cellulose crystallinity was determined also with solid-state NMR, yielding similar results as obtained with WAXS.

1.3.2 Lateral dimensions of cellulose crystals and fibrils

Microscopic techniques, such as transmission electron microscopy (TEM) or atomic force microscopy (AFM), can be used to obtain direct measures of the lateral dimensions of cellulose fibrils (Donaldson, 2007; Jakob et al., 1995). However, these methods suffer from a few limitations, namely, that they require complicated sample preparation procedures that alter the native sample structure and that they usually do not provide a reliable average of the whole sample (Jakob et al., 1995). In addition, it is often difficult to tell from an microscopy image whether the smallest observable units are individual cellulose microfibrils or bundles of them and whether they correspond to single crystals or to particles containing also less ordered components (Newman, 1999). These same challenges were met when interpreting the TEM images in paper **II** and the AFM images in paper **V** of this thesis, for which they were mainly used to obtain qualitative information and to support results obtained with other methods.

Indirect determination of lateral dimensions of cellulose crystals can be done with WAXS. The method is based on peak broadening due to the limited size of crystals (Cullity and Stock, 2001), which can be utilized to calculate a minimum value for the weight average of cellulose crystal size in different directions (Fink et al., 1995). The measured sample is typically of macroscopic dimensions, thus providing good statistics, and requires only minimal preparation prior to measurement (Jakob et al., 1995). Among the drawbacks of this technique are the influence of lattice distortions and the requirement of a non-trivial line shape for fitting (Fink et al., 1995; Jakob et al., 1995). Also a broad distribution of sizes complicates the analysis and may bias the results (Fink et al., 1995). In some cases, the crystal width can be overestimated due to less ordered cellulose or hemicellulose molecules on the crystal surfaces that have adopted a spatial ordering similar to that of the crystal interior chains (Driemeier et al., 2011; Fernandes et al., 2011). In this thesis, the lateral dimensions of cellulose

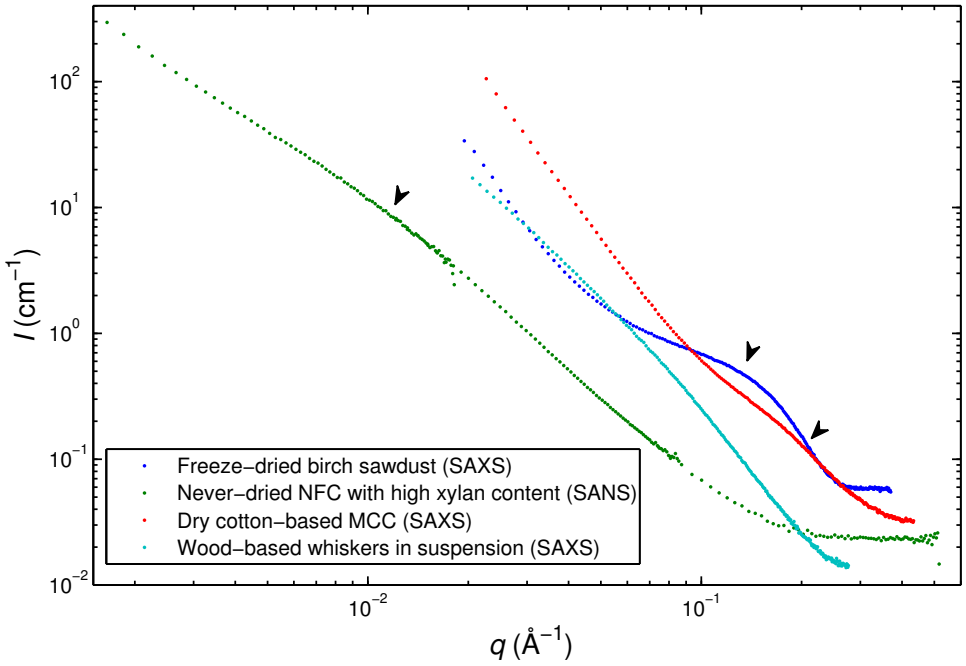

Figure 8. Small-angle x-ray and neutron scattering (SAXS and SANS) intensities of various cellulosic samples, with the arrowheads indicating shoulder features originating from the short-range order of cellulose microfibrils. The data has been taken from the papers.

crystallites were determined based on WAXS peak broadening in papers **I**–**III** and **V**.

The diameter of cellulose microfibrils can be estimated with small-angle scattering methods, which overcome the limitations of poor statistics of the microscopic techniques as well as some of the drawbacks related to WAXS (Jakob et al., 1995). On the other hand, small-angle scattering techniques are strongly dependent on the method applied to retrieve the information from the measured scattering intensities, in particular on the model chosen for fitting (Fernandes et al., 2011; Nishiyama, 2009). In some cases, interference peaks or shoulders arising from the centre-to-centre distance of parallel microfibrils may be observed directly (Fernandes et al., 2011) (Figure 8), but often fitting of a more or less complicated model is required to obtain the width of an individual cellulose microfibril (Jakob et al., 1995; Leppänen et al., 2009). Even though good agreement between the lateral fibril dimensions determined with small-angle scattering and crystal sizes obtained from WAXS intensities have been found in a number of studies (Fernandes et al., 2011; Jakob et al., 1995; Kennedy et al., 2007), also contradictory results, explained by occasional crystal aggregation, have been reported (Leppänen et al., 2009). A similar apparent discrepancy, i.e. a crystal width larger than the approximate distance between microfibril centre points, was also observed and discussed in papers **I** and **V** of this thesis, whereas good consistency was found between the results obtained in papers **III** and **IV**.

Sometimes also solid-state NMR is used to determine the lateral size of cellulose crystallites (Newman, 1999; Wickholm et al., 1998). This approach is based on the ratio of signals originating from the crystal interiors and from the surface chains as well as on the assumption that all of the cellulose contributing to the non-crystalline signal is located on the surfaces of crystals having a strict square cross-section. Despite the arguable assumptions, results obtained for various cellulosic samples have been relatively well in agreement with those obtained from peak broadening in WAXS (Kennedy et al., 2007; Newman, 1999; Wickholm et al., 1998). Also in paper **V** of this thesis the crystal sizes determined with NMR and WAXS were found to correspond well to each other.

1.3.3 Fibrillar packing and pore structure

Accessibility of cellulose plays a crucial role in many kinds of chemical and physical reactions. Especially for molecules or enzymes of nanometre dimensions, the physical structures formed by cellulose microfibrils may have a considerable limiting effect on this accessibility. Therefore, methods to characterize the nanometre scale morphology and packing of cellulose microfibrils and their bundles are highly desired. Some of these methods are discussed here briefly.

The most relevant methods for studying the nanoscale morphology of cellulosic substances regarding this thesis are the small-angle scattering methods, small-angle x-ray and neutron scattering (SAXS and SANS). These methods are based on the detection of regular or repetitive structures formed by inhomogeneities in the scattering length density relevant for each method. For instance the short-range order of cellulose microfibrils produces certain features in the scattering intensities (Figure 8), which are affected by the shape of the structures as well as their locations related to each other and the scattering length density contrast between them. Similarly, the pores and interfaces between microfibrils and their bundles scatter x-rays and neutrons, bringing their own contribution to the scattering intensities. As these contributions often overlap each other, the interpretation of small-angle scattering intensities from biomass-based samples can be rather complicated. The methods used for obtaining information from small-angle scattering intensities will be described in more detail in the next chapter, but here one of the extractable quantities, the specific surface area, is briefly introduced.

The specific surface area of a material represents its total surface area per a unit of mass. It can be determined for instance by adsorption measurements, which utilize water vapour or an inert gas like nitrogen (N_2) to measure the available surface area for adsorption. The surface area is obtained from an adsorption isotherm, which relates the fractional coverage of the available adsorption sites in the material to the pressure of the gas at a certain temperature (Atkins and de Paula, 2010). The interpretation of the adsorption isotherm requires a model, where the Brunauer-Emmett-Teller (BET) model is often chosen for cellulosic samples (Kocherbitov et al., 2008). Water vapour

sorption is suitable for determining the areas accessible for water, including some of the spaces between microfibrils, whereas N_2 adsorption measurements are carried out in dry state and are therefore more descriptive of the outer surface area of larger particles (Kocherbitov et al., 2008). Another potential method for the determination of wet surface area is thermoporosimetry, which also yields the pore size distribution of the material (Pönni et al., 2012). This method is based on observing the depression of the precise melting temperature of a solvent of a certain molecule size, which depends on the surface energy at the solid–liquid interface and therefore also on the pore size. Also solid-state NMR has been shown to be capable of determining the specific surface area in pulp samples (Chunilall et al., 2010; Larsson et al., 2013). In general, care should be taken when comparing specific surfaces determined with different methods, because the size of the probe and the surface area available for them may be significantly different. Nevertheless, values in the order of 1 m^2/g are generally to be expected for dry MCC samples (N_2 adsorption) and 100 m^2/g for wet samples (water adsorption) (Kocherbitov et al., 2008).

As already mentioned, small-angle scattering can also be applied to measure the specific surface area of a material and, in principle, it can be done for both wet and dry samples (Porod, 1982; Spalla et al., 2003). The specific surface determination with small-angle scattering is based on the properties of the scattering intensity related to the total interfacial area between the phases of a two-phase system. In this thesis, SAXS was used to determine the specific surface of various cellulosic materials in papers **I**, **II**, and **V**, and the results were compared to values obtained with other methods.

2 Materials and methods

2.1 Materials

Various cellulosic materials related to different steps of the biorefining process (Figure 1) were the subject of study in this thesis. These materials and their preparation are presented only briefly in this section, whereas more detailed descriptions can be found in each paper separately. Also the motivations behind using these particular materials in the different studies have been discussed in the publications.

2.1.1 Pretreated birch sawdust (paper I)

Pressurized hot water extraction with a flow-through system was used to extract hemicelluloses and lignin from birch sawdust with different particle sizes and packing densities. The freeze-dried extraction residues consisting of cellulose and residual hemicelluloses and lignin were examined for structural changes in various length scales using WAXS, SAXS, and x-ray microtomography. The reference samples of untreated sawdust included also a never-dried sample that was characterized with SAXS. Within this thesis, the birch sawdust samples can be considered to represent the native structure of wood, consisting of fibrillar cellulose in a hemicellulose–lignin matrix.

2.1.2 Substrates and residues of enzymatic hydrolysis (papers II–IV)

The limiting factors of the enzymatic hydrolysis of cellulose for biofuels production were investigated using two different model systems, microcrystalline cellulose (MCC) (paper **II**) and nanofibrillated cellulose (NFC) with varying xylan content (papers **III** and **IV**). Produced from pulp by acidic hydrolysis, the MCC represented a purely cellulosic material with remaining microfibril bundles and a relatively high crystallinity, whereas the NFC consisted of separated fibrils with somewhat lower crystallinity and a considerable proportion hemicellulose. Commercial MCC (Avicel) was used in paper **II** as such and subjected to hydrolysis by an enzyme mixture from the fungus *Trichoderma reesei*. After hydrolysis to various degrees, the solid residue of the hydrolysis was collected and freeze-dried for the x-ray analyses. To obtain the NFCs with varying xylan content for papers **III** and **IV**, bleached birch kraft pulp was treated with xylanase enzyme to produce pulps with reduced xylan contents. The original as well as the xylanase-treated pulps were mechanically fibrillated to NFC and the NFCs with highest and lowest xylan content were hydrolysed to various degrees by an enzyme mixture. Part of the hydrolysis residues were used to prepare thin films for the dynamic FT-IR spectroscopy and WAXS measurements of paper **III**, whereas the rest were used in wet state in the SANS and SAXS measurements of paper **IV**.

2.1.3 Cellulose whiskers (paper V)

Cellulose whiskers were prepared from MCCs based on cotton linters and wood pulp by hydrolysing them in sulphuric acid, after which part of the suspensions were neutralized with NaOH. In order to study the effects of different drying conditions on the resulting structures, the suspensions were dried by freeze-drying, with or without melting in between, or in air at ambient conditions. The whisker suspensions were analysed with SAXS and the differently dried whiskers with SAXS, WAXS, solid-state NMR, and FT-IR spectroscopy. The whiskers were the most rigorously treated cellulosic material studied in this thesis, thereby presenting a possible end product of the biorefining process.

2.2 Methods

This section outlines the theoretical framework for elastic scattering of x-rays and neutrons, after which the particular methods used in this thesis are described and discussed in more detail. Finally, brief presentations of a few other physical characterization methods used in this work are given. The descriptions of the specific measurement setups and other experimental details, including the exact data treatment procedures, can be found in the original papers.

2.2.1 Theoretical background for scattering

X-rays are electromagnetic radiation with wavelength in the order of 1 Å (0.1 nm = 10^{-10} m). They can be generated by x-ray tubes, where electrons are accelerated by a high voltage to hit a target material, causing ionization of the target atoms and leading to the production of an x-ray spectrum with characteristic peaks accompanied by a continuous distribution arising from the rapid deceleration of the electrons. More intense x-ray beams can be produced by synchrotrons, where electrons or positrons emit x-ray radiation while subjected to centripetal acceleration in magnetic fields. The scattering applications of this thesis use monochromatic radiation, which can be separated from the broader spectrum using a specially constructed monochromator. The x-ray radiation used for the scattering experiments of this thesis was mostly obtained from laboratory sources with a Cu Kα anode (papers **I**–**III** and **V**), except for paper **IV**, where synchrotron radiation was employed.

X-ray photons can interact with matter either by photoabsorption or scattering (Als-Nielsen and McMorrow, 2001). In photoabsorption, the incoming x-ray photon transfers all of its energy to an orbital electron of the absorbing atom, whereby the electron is expelled and the atom becomes ionized. As for the case of scattering by an electron, the photon may either retain all of its energy or lose part of it to the electron. When the energy of the x-ray photon is preserved, the process is called

elastic scattering, which is the most relevant interaction exploited by the scattering methods applied in this thesis. According to the classical picture of elastic scattering of x-rays by electrons, i.e. Thomson scattering, the electric field of the incoming x-ray forces an electron in oscillatory motion, which generates a spherical wave. The scattered spherical wave has the same frequency as the incoming photon, but its phase has been shifted by 180°. As the incoming wave is simultaneously scattered from several electrons in the sample, the coherently scattered spherical waves interfere with each other in a way that is determined by the relative positions of the electrons and their host atoms. The alternative case, where the photon transfers part of its energy to the electron during the scattering incident, is referred to as inelastic x-ray scattering. In contrast to the elastic Thomson scattering, inelastic scattering is incoherent, meaning that the frequency and phase of the emitted photon are different from those of the incident photon.

Due to the concept of wave–particle duality, neutrons are also scattered by matter and they may therefore be employed in scattering studies (Bacon, 1977). Neutrons having an appropriate wavelength can be produced at nuclear research reactors. In the process, neutrons are released by nuclear fission reactions and slowed down to the desired speed by a moderator medium such as liquid deuterium. The neutrons used for small-angle scattering are so-called cold neutrons, which have their de Broglie wavelength in the same scale as the electromagnetic wavelength of x-ray photons, i.e. typically between 1 and 20 Å. Before hitting the sample, the neutrons are monochromatised by a velocity selector and collimated with apertures. The principles underlying the scattering of neutrons by non-magnetic matter are based on strong force interactions with the nuclei of the scattering medium. The range of this force is so small compared to the wavelength of the neutrons, that the nucleus can be considered as a point scatterer. In this thesis, neutron scattering was applied in paper **IV** and the results were compared to those obtained with x-ray scattering.

Despite their different mechanisms, the scattering of x-rays and neutrons can be mathematically described in a similar way. The differential scattering cross-section per unit sample volume $\frac{d\Sigma}{d\Omega}$, which represents the probability of a photon or neutron being scattered by a unit sample volume into the solid angle element $\Delta\Omega$, can be expressed as

$$\frac{d\Sigma}{d\Omega} = \frac{1}{V} \cdot \frac{IR^2}{I_0}, \tag{1}$$

where V is the unit sample volume (cm^3), I_0 the intensity of the incoming beam, and R is the distance (cm) between the scatterer and the detector pixel that measures the scattered intensity I (Lindner, 2002). Here the cross-sectional area of the incident photon or neutron flux is assumed to be smaller than that of the sample and the intensity is expressed as the number of photons or neutrons flowing through a unit area per second. The unit of $\frac{d\Sigma}{d\Omega}$ is cm^{-1} and it is referred to as the scattering intensity

in absolute units in papers **I**, **II**, **IV**, and **V** of this thesis.

In elastic scattering (Feigin and Svergun, 1987), the amplitude of the scattered wave $A(\mathbf{q})$ can be obtained by integrating over all of the individual scatterers in the sample, which yields

$$A(\mathbf{q}) = \int \rho(\mathbf{r}) e^{i\mathbf{q}\cdot\mathbf{r}}\, d\mathbf{r}. \tag{2}$$

Equation 2 is essentially a Fourier transform of the scattering length density $\rho(\mathbf{r})$ in the sample. For the scattering of x-rays, the scattering length density $\rho(\mathbf{r})$ is proportional to the number of electrons per unit volume (electron density), whereas for neutrons it corresponds to the density of the scattering lengths of the nuclei. The neutron scattering lengths are different for each nucleus and they may be positive or negative, however, unlike the x-ray scattering amplitude of a neutral atom (atomic scattering factor), they do not depend on the scattering angle. The scattering vector $\mathbf{q}$ appearing in Equation 2 is defined as $\mathbf{q} = \mathbf{k} - \mathbf{k}_0$, where $\mathbf{k}_0$ and $\mathbf{k}$ are the incident and scattered wave vectors, respectively, separated by the scattering angle 2θ. For elastic scattering $|\mathbf{k}_0| = |\mathbf{k}|$ and the magnitude of the scattering vector is

$$|\mathbf{q}| = \frac{4\pi \sin(\theta)}{\lambda}, \tag{3}$$

where θ is half of the scattering angle and λ is the wavelength of the incoming x-rays or neutrons. The intensity I of the scattered wave in Equation 1 is proportional to the absolute square of the scattering amplitude of Equation 2:

$$I(\mathbf{q}) = |A(\mathbf{q})|^2. \tag{4}$$

2.2.2 Wide-angle x-ray scattering

For an infinite set of point-like scatterers (atoms) organized in a periodic crystal lattice defined by the set of lattice vectors

$$\mathbf{R}_n = n_1\mathbf{a}_1 + n_2\mathbf{a}_2 + n_3\mathbf{a}_3 \tag{5}$$

with $\mathbf{a}_i$ being the basis vectors of the lattice and n_i integers, the scattering amplitude $A(\mathbf{q})$ of Equation 2 reduces to a sum of discrete nonzero values corresponding to definitive values of $\mathbf{q}$ (Als-Nielsen and McMorrow, 2001). These values, which also determine the positions of the intensity peaks observable in an x-ray diffraction or WAXS experiment, are defined by the Laue condition

$$\mathbf{q} = \mathbf{G}_{hkl} = h\mathbf{b}_1 + k\mathbf{b}_2 + l\mathbf{b}_3. \tag{6}$$

The vectors $\mathbf{b}_i$ in Equation 6 are the reciprocal basis vectors corresponding to the basis vectors $\mathbf{a}_i$ in real space and the indices h, k, and l are the Miller indices, which define the plane of reflection in the crystal lattice. The direction of these planes is perpendicular to the vector $\mathbf{G}_{hkl}$ and they are placed at intervals of

$$d_{hkl} = \frac{2\pi}{|\mathbf{G}_{hkl}|}. \tag{7}$$

The locations of the diffraction peaks at the positions dictated by Equation 6 are preserved also in the case of a crystal of limited size. However, the destructive interference at positions close to the value of $\mathbf{q}$ that fulfils the Laue condition (Equation 6) is incomplete, which leads to broadening of the intensity peak (Cullity and Stock, 2001; Klug and Alexander, 1974). The extent of the peak broadening can be related to the size of the crystal L_{hkl} in the direction perpendicular to the lattice plane (hkl), which is expressed by the Scherrer equation

$$L_{hkl} = \frac{K\lambda}{\Delta 2\theta \cos\theta}. \tag{8}$$

The broadening of the diffraction peak corresponding to reflection hkl is described in Equation 8 by its full-width at half maximum (FWHM) $\Delta 2\theta$, whereas the angle θ is equal to the Bragg angle of the reflection (half of the scattering angle 2θ). The value of the constant K, which has been chosen here as 0.9, depends on the shape of the crystal and the definitions of L_{hkl} and $\Delta 2\theta$. The additional peak broadening caused by deviations from the ideal case of a parallel and monochromatic x-ray beam and an infinitely thin sample, i.e. the instrumental effect $\Delta 2\theta_{inst}$, can be taken into account by assuming Gaussian peak profiles and substituting $\Delta 2\theta$ with $\sqrt{(\Delta 2\theta)^2 - (\Delta 2\theta_{inst})^2}$ in Equation 8. This form of the Scherrer equation was applied to calculate the crystallite dimensions in papers **I**–**III** and **V** of this thesis. The specific procedures to obtain the peak widths from the experimental WAXS intensities have been described particularly in papers **I** and **II**.

The crystallinity of a semicrystalline polymer can be estimated from its WAXS intensity, for which various methods are available (Section 1.3.1). In this work, the sample crystallinity, meaning the proportion of crystalline cellulose in the sample, was determined by fitting the WAXS intensities with an experimentally determined amorphous background (sulphate-lignin) together with a number of Gaussian functions corresponding to different reflections of cellulose Iβ (Nishiyama et al., 2002). The crystallinity CrI was obtained by using the equation

$$CrI = 1 - \frac{\sum I_{am}}{\sum I_{tot}}, \tag{9}$$

where $\sum I_{am}$ is the integrated intensity of the scaled amorphous background and $\sum I_{tot}$

the total integrated intensity of the measured sample. This method for crystallinity calculations has been described in more detail in papers **I** and **II** and applied in papers **I**–**III** and **V** of this thesis. Paper **I** also shortly discusses the results obtained with this method as compared to the Segal method mentioned in Section 1.3.1.

2.2.3 Small-angle x-ray and neutron scattering

Disperse systems having a low degree of order do not produce diffraction peaks like those arising from crystals in WAXS. Nevertheless, these kind of samples may show spatial correlations and regular inhomogeneities in a scale larger than the interatomic distances. These features may be related for instance to particle shapes, surface structures, or short-range order in the nanometre scale or above. Due to their larger dimensions compared to the interatomic distances, these inhomogeneities contribute to the scattering on the area around the direct beam in scattering experiments applying wavelengths in the order of 1 Å, for which reason the corresponding scattering method is referred to as small-angle scattering. As described in Section 2.2.1, the scattering particles can be either photons, as in small-angle x-ray scattering (SAXS), or neutrons, as in small-angle neutron scattering (SANS), but in both cases similar methods may be applied to interpret the scattering data. Small-angle scattering methods were mentioned already in Sections 1.3.2 and 1.3.3 in relation to cellulosic samples and here the discussion is continued on a more general level.

For a system consisting of several phases with different scattering length densities, perhaps the most relevant property regarding small-angle scattering is the absolute difference of the scattering length density between the phases (Feigin and Svergun, 1987; Porod, 1982). In principle, this scattering length density contrast determines to which extent the different phases and features contribute to the scattering. This fact can be applied to achieve selectivity in the scattering by tuning the scattering length density for instance of the solvent in a sample in liquid, as is done in the contrast variation method of SANS, applied in paper **IV**. For the sake of simplicity, an assumption of a two-phase system, dictated by the largest possible contrast, is typically made when interpreting small-angle scattering data. Referring to the short discussion given in paper **II**, these two phases were assumed as solid material and air in dry cellulosic samples (papers **I**, **II**, and **V**) and as cellulose crystals and water in wet samples (papers **I**, **II**, **IV**, and **V**) throughout this thesis.

In the case of a two-phase system with smooth but sharp interfaces between domains of homogeneous scattering length density, the asymptotic behaviour of the small-angle scattering intensity on large q values can be shown to follow a power law of the form

$$I(q) \propto q^{-\alpha} \tag{10}$$

with $\alpha = 4$, commonly known as the Porod law (Feigin and Svergun, 1987; Porod,

1982). This behaviour of intensity is related to the total area of the interface between the two phases and it can therefore be used to calculate the specific surface of the sample. The surface-to-volume ratio S/V of the sample can be obtained from the equation

$$\frac{S}{V} = \frac{\lim_{q\to\infty} q^4 \frac{d\Sigma}{d\Omega}(q)}{2\pi(\Delta\rho)^2}, \tag{11}$$

where $\Delta\rho$ represents the scattering length density contrast between the two phases and $\frac{d\Sigma}{d\Omega}$ is the intensity on absolute scale (Equation 1). A more detailed description of the procedure to obtain the specific surface, i.e. the total surface area per a unit of mass, of a sample from experimental SAXS data can be found in the supporting material of paper **II**. This method was applied in papers **I**, **II**, and **V** to determine specific surface areas in cellulosic samples, including both dry and wet samples.

If the scattering intensity obeys a power law of the form of Equation 10 with a non-integer α, the data can be interpreted based on fractal geometry (Schmidt, 1991). In general, fractals are structures showing self-similarity in all scales, which is certainly not possible for a real object. However, for physical structures, fractal properties may be found within a limited spatial range, which in an optimal case covers several orders of magnitude. Two types of fractal systems can be considered, namely, mass fractals and surface fractals. For a system with mass fractal dimension D_m, the mass $M(r)$ confined inside a sphere with radius r and centre at the mass fractal centre obeys the proportionality

$$M(r) \propto r^{D_m}. \tag{12}$$

For normal mass fractal systems with fractal properties extending throughout the system, the value of the mass fractal dimension is below three, i.e. $D_m < 3$, whereas the integer value $D_m = 3$ corresponds to the limiting case of a dense system filling the three-dimensional Euclidean space completely. Surface fractals, on the other hand, are defined as systems that are dense inside (with $D_m = 3$) but bounded by a fractal surface with surface fractal dimension D_s. The surface fractal dimension D_s can have values in the range $2 \leq D_s \leq 3$. A relation between the fractal dimension and the small-angle scattering intensity $I(q)$ of a system can be found, when q fulfils the condition $q\xi \gg 1$, where ξ is a length characterizing the size of the structures producing the scattering. In this case, a mass fractal system obeys the power law of Equation 10 with $\alpha = D_m$ and a surface fractal system in the Euclidean space that with $\alpha = 6 - D_s$. The fractal interpretation of small-angle scattering data was applied in papers **I**, **II**, **IV**, and **V** to characterize the fibrillar structure and surface morphology of the materials.

2.2.4 Other methods

X-ray microtomography

X-ray microtomography is a computed tomography (CT) imaging method, which is based on the absorption of x-rays while transmitting the sample (Hsieh, 2009). During an x-ray microtomography measurement the sample is rotated and imaged in an x-ray beam having a wide cross-section and the projection images formed by the transmitted beam are measured for a large number of angles. The projections are combined using a computerized backprojection algorithm to yield a three-dimensional reconstruction of the sample, where the grayscale value of each voxel is proportional to the linear x-ray attenuation coefficient of the corresponding micrometre-sized volume in the real sample. In this thesis, x-ray microtomography was used to observe the micrometre scale structure of cellulosic samples in papers **I** and **II**. In paper **I** image analysis was applied to the reconstructions to compute the wall thickness of wood fibres.

FT-IR spectroscopy

Infra-red spectroscopy is based on observing the absorption of infra-red radiation on certain frequencies, which correspond to the normal modes of vibration in the molecules of the sample (Atkins and de Paula, 2010; Gedde, 1995). The infra-red active modes of vibration are related to oscillating electric dipoles, where the frequency of oscillation is specific to each dipole in a certain environment, including bond lengths and bond angles. In case of a sample with preferred orientation, polarized infra-red radiation can be applied to evoke vibrations in the plane of the polarization, which enables better separation of signals from differently oriented vibrations and opens up the possibility for orientational studies. Fourier-transform infra-red (FT-IR) spectroscopy owes its full name to the fact that a Fourier-transform is applied to extract the different frequency components from the recorded net absorption, obtained by irradiating the sample with a set of wavelengths simultaneously. FT-IR spectroscopy was applied in papers **III** and **V** of this thesis to study the molecular structure of cellulosic samples. A more recently developed method, dynamic FT-IR spectroscopy, was used in paper **III** to study the orientation and interactions of cellulose and xylan. In this method, a small oscillatory strain is used to exclusively detect the vibrations connected to the external perturbation and to each other.

Solid-state NMR

Nuclear magnetic resonance (NMR) is a spectroscopic method, where the transitions of nuclear spin in a strong external magnetic field are observed using radiofrequency radiation (or vice versa) (Atkins and de Paula, 2010; Gedde, 1995). The resonance frequency of the transition depends on the local surroundings of the particular nucleus (such as ^{13}C), including for instance hydrogen bonding interactions, which introduce a difference called chemical shift between the observed frequency and a reference value.

In magic-angle spinning (MAS) NMR the solid sample is spun at a kilohertz frequency with the spinning axis at an angle of 57.74° to the applied magnetic field (magic angle), which reduces the line broadening due to anisotropic dipole–dipole interactions that are automatically averaged by random motion in the case of liquid samples. In this thesis, ^{13}C CP/MAS NMR was used to study the cellulose crystal structure and crystallinity in paper **V**.

3 Results and discussion

This section summarizes the key results of each paper, paying special attention to those obtained with x-ray and neutron scattering methods. More detailed discussion on each topic and the relevance of the results in the field of the specific research problems can be found in the corresponding papers. The section is concluded by some general observations in the context of structural characterization of cellulosic materials, referring to the topics of Section 1.3.

3.1 Pressurized hot water extraction of sawdust (paper I)

The aim of paper **I** was to investigate the structural changes taking place in the submicrometre structure of birch sawdust when subjected to pressurized hot water extraction. In the extraction, over 80% of the original hemicelluloses and about 50% of the lignin were removed, whereas the cellulose content remained practically unchanged. The DP of both cellulose and hemicelluloses, however, was clearly reduced. The cellulose crystal size, calculated with the Scherrer equation (Equation 8) from the 200 reflection of cellulose Iβ from WAXS measurements with two different geometries, showed an increase by about 30% (Table 1). The obtained crystal sizes from the measurements in perpendicular transmission geometry were slightly larger than those determined in symmetrical reflection geometry, which was primarily explained by differences in the fitting methods used to subtract the amorphous background and to determine the peak width. The sample crystallinity was observed to increase from 24 to 30%, but when taking the cellulose content into account, an opposite trend with slightly decreased crystallinity was revealed (Table 1). SAXS was used to discover changes in the fibrillar ordering and pore structure. The increased specific surface area (Table 2) suggested that new surfaces were revealed during the treatment. This conclusion was further supported by the rougher pore surfaces in the extracted samples, indicated by an increased surface fractal dimension, and by the denser association of microfibrils, which was evidenced by a shift of the shoulder feature in the logarithmic intensity plots to larger q values (Figure 4 in paper **I**). The shift appeared even more pronounced, when the intensity was plotted as a Kratky plot ($q^2I(q)$ vs. q, Figure 6 in paper **I**). The x-ray microtomography images clearly demonstrated a reduction in the fibre cell wall thickness. A noteworthy result not directly related to the pressurized hot water treatment, was that the freeze-drying of birch sawdust did not affect the distance between microfibrils, as shown by the preserved location of the peak in the Kratky plot of the SAXS intensities (Figure 6 in paper **I**).

In paper **I**, the results could be explained in the framework of the nanoscale structure of native wood, discussed in Section 1.2.3 and illustrated in Figure 8 of paper **I**. Even though the observed increase in the crystal width appears contradictory to the reduced interfibrillar distance, it should be kept in mind that the SAXS results represent

Table 1. Cellulose crystal sizes and crystallinities determined with WAXS for various materials.

Sample	Source	L_{hkl}[a] (nm)				CrI_S[b] (%)	CrI_C[c] (%)	Paper
		1-10	110	200	004			
Sawdust[d]	Birch wood	–	–	3.2	–	24	60	**I**
Hot-water treated sawdust	Birch wood	–	–	4.3	–	30	45	**I**
MCC (Avicel, Serva 14204)	Unknown	5.0	5.0	5.3	–	48	–	**II**
Enzymatically hydrolysed MCC	MCC (Avicel, Serva 14204)	4.7–4.8	5.5–5.7	5.2–5.4	21–24	49–50	–	**II**
NFC with original xylan content	Birch kraft pulp (BKP)	–	–	4.0	–	43	56	**III**
NFC with low xylan content[d]	BKP treated with xylanase	–	–	4.1	–	48	55	**III**
Enzymatically hydrolysed NFC	NFC from BKP	–	–	4.5–4.6	–	52–57	72–85	**III**
Enzymatically hydrolysed NFC	NFC from xylanase-treated BKP	–	–	4.6–4.7	–	49–54	57–62	**III**
Cellulose whiskers[d] and MCC[d]	MCC from cotton linters/wood pulp	3.7–4.7		5.2–5.5	19–22	50–58	–	**V**

[a] Cellulose crystal size determined with Equation 8 from reflection hkl.
[b] Sample crystallinity calculated using Equation 9.
[c] Cellulose crystallinity estimated from CrI_S based on cellulose content.
[d] WAXS intensity plotted in Figure 7.

Table 2. Specific surface area determined with SAXS for various materials.

Sample	Source	Specific surface area[a] (m^2/g)	Paper
Sawdust (freeze-dried)	Birch wood	0.19–0.87	**I**
Hot-water treated sawdust (freeze-dried)	Birch wood	3.3–4.9	**I**
Enzymatically hydrolysed MCC (freeze-dried)	MCC (Avicel, Serva 14204)	3.3–3.6	**II**
Enzymatically hydrolysed MCC (rewetted freeze-dried)	MCC (Avicel, Serva 14204)	220–410	**II**
MCC (dry)	Cotton linters and wood pulp	7–8	**V**
Cellulose whiskers (air-dried)	MCC from cotton linters/wood pulp	3–4	**V**
Cellulose whiskers (freeze-dried)	MCC from cotton linters/wood pulp	4–25	**V**

[a] Determined with Equation 5 in the supporting material of paper **II**.

a better average of the sample, unlike the biased crystal width obtained from the peak broadening in the WAXS intensities. Therefore, the crystal width determined with WAXS was thought to emphasize the larger crystals, possibly formed by occasional aggregation, whereas the SAXS intensities would give a more reliable overall picture of the structure. Even though the interfibrillar distance determined with SAXS cannot be held as absolutely correct, because it was simply determined from the peak position in the Kratky plot without using any model for fitting, the trend of denser packing of individual microfibrils in the treated samples was obvious. The values of cellulose crystallinity, on the other hand, were very sensitive to small deviations in the sample composition and the sample crystallinity, which complicated their interpretation. In any case, it seems plausible that the crystallinity of cellulose did not increase in the pressurized hot water treatment, but rather decreased or remained unchanged. An opposite trend has been reported in some studies Hu and Ragauskas (2012), but at least a part of them have used less accurate techniques like the Segal method (Section 1.3.1) for the determination of crystallinity. Also differences in the raw material and the treatment conditions may lead to wide variation in the resulting properties of the residue (Mosier et al., 2005; Pedersen and Meyer, 2010). From the biorefinery point of view, the extraction residue of birch sawdust represents a potential substrate for enzymatic hydrolysis or a raw material for dissolving pulp applications. For both applications, however, further delignification would seem necessary.

3.2 Enzymatic hydrolysis of cellulose (papers II–IV)

The studies presented in papers **II**–**IV** are all related to the topic of enzymatic hydrolysis of lignocellulose and they share the aim of understanding the structural factors that limit this process. In these papers, several of the limiting factors were investigated, including morphological aspects and hemicellulose content.

The system under study in paper **II** was commercial MCC, which was hydrolysed to various degrees. As already the original dry MCC consisted of heterogeneous particles of tightly packed bundles of microfibrils (Moon et al., 2011), the most easily accessible portion of the substrate was degraded first, leaving particles less accessible to the enzymes behind (Figure 9a). Therefore, all of the studied hydrolysis residues contained a considerable proportion of recalcitrant aggregated structures, which governed the observed properties of the samples. This was how the unchanged crystallinity and crystal size observed with WAXS (Table 1) could be explained. The remaining larger structures seen in the transmission electron microscopy (TEM) images as well as the roughly preserved nanoscale properties, such as the specific surface area (Table 2), were also in line with this picture. Besides a decrease in particle size in the micrometre scale, observed with x-ray microtomography, the only detectable changes in the structure of the residue were found with SAXS in rewetted samples. The change in the shape of

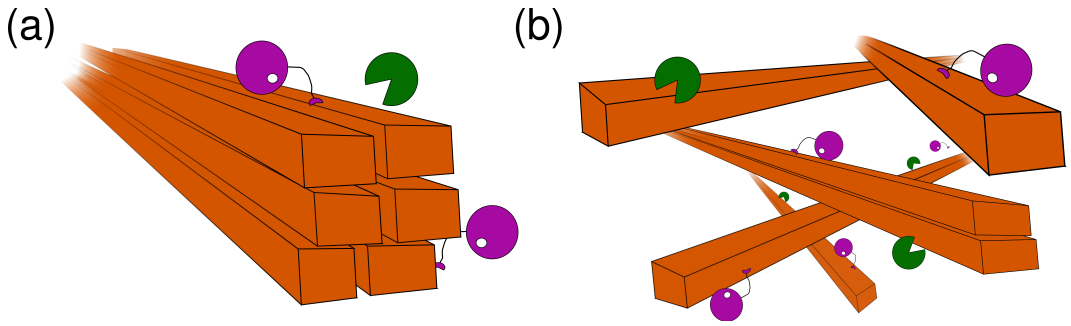

Figure 9. Illustrative representation of the enzymatic hydrolysis of (a) microcrystalline cellulose (MCC) and (b) nanofibrillated cellulose (NFC).

the SAXS curve was quantified by a power law fit, where a decrease of the mass fractal dimension was interpreted to be caused by modest loosening of the microfibril bundles. This observation led to the conclusion that in order to find out the true changes caused by the enzymes to the morphology of the microfibril bundles, drying of samples after the hydrolysis should be avoided.

In papers **III** and **IV** the substrate for the enzymatic hydrolysis consisted of NFC made of birch pulp with varying xylan content, which was obtained by specific hydrolysis of xylan prior to mechanical fibrillation. Two slightly different perspectives were adopted in the two papers studying the NFCs and their hydrolysis residues, namely, that of the molecular scale structure and interactions of cellulose and xylan (paper **III**) and that of the nanoscale structure of the microfibril network (paper **IV**). The advantage of this system, as compared to that of paper **II**, was that in this case the cellulose fibrils and microfibrils were separated from each other prior to the enzymatic hydrolysis, thereby minimizing the influence of fibrillar aggregation (Figure 9b). Another benefit of the choice of material was that the nanoscale structure of the original substrate and the hydrolysis residues could be studied in never-dried state using neutron and x-ray scattering techniques (paper **IV**).

In the results of the NFC hydrolysis (paper **III**), it was clear that the presence of xylan limited the enzymatic hydrolysis of cellulose also. In the NFC with original xylan content, both the cellulose crystallinity and crystal size increased during the hydrolysis (Table 1), indicating that the presence of xylan either hindered the hydrolysis of crystalline cellulose in particular or favoured the crystallization of cellulose chains on the crystal surface after partial hydrolysis. Lateral aggregation of crystals could also explain the observed effects. In any case, the dynamic FT-IR measurements showed that a fraction of xylan was attached to the cellulose crystals in a parallel fashion and that this fraction remained attached during the enzymatic hydrolysis also. The SANS and SAXS results of paper **IV** were in line with the molecular scale changes, demonstrating with the aid of an empirical model that the microfibril network retained its short-range shape during the hydrolysis, when the xylan was not removed prior to

the cellulase hydrolysis. This could also be observed as a preserved peak in the Kratky plots of the SANS and SAXS intensities, which was their only characteristic feature besides a power law with mass fractal dimension between 2 and 3. In the hydrolysis series of the NFC with reduced xylan content, cellulose and xylan were hydrolysed concomitantly, leading to the preservation of cellulose crystallinity in the beginning of the hydrolysis and a gradual disruption of the crystals at later stages, as detected with WAXS (paper **III**). At the same time the nanoscale microfibrillar network was loosened and broken down, which was seen in the SANS and SAXS experiments as a shift of the weakening Kratky-plot peak towards smaller q values (Figures 5 and 6 in paper **IV**). Even though the limiting role of xylan could be clearly demonstrated, the hydrolysis in both sample series was eventually limited by other factors. These were speculated in paper **IV** to be related to some of the more resistant parts of the heterogeneous NFC, involving also larger structures. As an additional result obtained with dynamic FT-IR in paper **III**, the fraction of xylan tightly attached to cellulose was observed in the NFC with reduced xylan content also, indicating that the xylanase pre-hydrolysis primarily removed the more loosely bound fraction of xylan from the birch pulp.

To consider the results of papers **II**, **III**, and **IV** in a broader context, a particularly interesting point of view is that of the cellulose crystallinity. The role and behaviour of cellulose crystallinity in the enzymatic hydrolysis of lignocellulose has represented an unsolved puzzle already for years (Bansal et al., 2012; Cateto et al., 2011; Mansfield et al., 1999; Park et al., 2010). The various results showing both increased and decreased crystallinities appear contradictory to each other, although part of them may be explained by the challenges related to the accurate experimental determination of cellulose crystallinity (Section 1.3.1). Lately, the importance of the nanoscale sample morphology and its determining role to the enzyme accessibility have been better recognized (Arantes and Saddler, 2010; Bubner et al., 2013; Fink et al., 1992; Mansfield et al., 1999). In particular, some recent observations related to the synergy of the different cellulases (Ganner et al., 2012; Jalak et al., 2012) offer new insights to the traditional picture presented in Figure 6 (Section 1.2.4) and support the conclusions of papers **II** and **III**. Ganner et al. (2012) used atomic-force microscopy (AFM) to visualize the action of the different cellulase enzymes on the structure of a model substrate consisting of an amorphous matrix embedded with large crystals and smaller fibril-like crystalline units. They found out that the amorphous and less ordered regions were degraded by EG and CBH II to uncover the fibril-like crystals, which were rapidly hydrolysed by the introduction of CBH I. One would expect a similar mechanism to work also in more complex substrates, which still possess the fibril structures characteristic of native wood (Section 1.2.3). For that kind of natural-like substrate, the access of the different enzymes to their preferred binding sites would be restricted by the complex structure formed by the tightly packed cellulose microfibrils, probably also surrounded by hemicelluloses. Thus, in order to be able to hydrolyse their way to the bulk of

the substrate, synergistic action of all of the enzymes is required. Along with this picture, one could speculate that the function of CBH II in a natural substrate would be to remove the less ordered surface chains on the cellulose microfibrils to expose the crystallite surface to CBH I, which would be able to proceed along the obstacle-free crystal surface and hydrolyse it efficiently. Also some recrystallization of the partly hydrolysed surface chains might take place, similarly to mild acid hydrolysis (Battista, 1950), which could be a possible cause for the increased crystallinity and crystal size detected for the NFC samples with original xylan content in paper **III**. A possible role of EG, on the other hand, could be to attack the small amorphous regions in the longitudinal direction of the fibrils (Nishiyama et al., 2003), thereby loosening the fibrillar aggregation and reducing the DP of cellulose to the same order as the levelling-off DP discussed in Section 1.2.4 (Kleman-Leyer et al., 1996; Zhang and Lynd, 2004).

3.3 Drying of cellulose whiskers (paper V)

The work presented in paper **V** focused on the effects of two commonly used drying methods, freeze-drying and air-drying, on the nanoscale structure and thermal properties of cellulose whiskers. The aim of the study was to characterize the resulting structures and to elucidate the factors related to their formation during drying as well as their degradation during heating. The effects of surface charge neutralization prior to drying were also addressed.

The results of both WAXS and solid-state NMR analyses showed that the crystallinity and crystal size of the whiskers did not differ from those of MCC (Table 1), with the values of both crystallinity and crystal width being relatively well in agreement between the two methods. The clear differences in the macroscopic structure and in the thermal behaviour were therefore thought to be linked to the charged surfaces and to the nanoscale packing of the whiskers, in which the surface charges also affected the drying behaviour and the resulting morphology. The most prominent differences in the nanoscale structure observed with SAXS were related to the strength of the shoulder arising from the short-range order of cellulose fibrils, which was only seen in the whiskers having their surface covered by negatively charged sulphate groups (Figure 7 in paper **V**). The neutralization of these charges led to a weakening of the shoulder, indicating less regular packing than in the non-neutralized whiskers, and this effect was more pronounced in the samples dried at ambient conditions than by freeze-drying. These trends were also reflected in the specific surface area, which was slightly lower for the air-dried samples (Table 2). Whiskers prepared from cotton MCC showed better short-range order of the microfibrils than those based on wood MCC, but no other differences were observed between the two raw materials.

In general, an increase in the crystallinity of cellulose during whisker preparation would be expected due to the removal of the amorphous fractions by the acid hydrolysis

(Moon et al., 2011). However, the results of paper **V** clearly showed that the change from the original MCC was negligibly small, if any. Even though the NMR analysis yielded crystallinity values a few percentage points smaller for the MCC and neutralized whiskers than for the non-neutralized whiskers, no such consistent trend could be observed with WAXS. The preservation of the crystallinity might be explained by the increased proportion of surface chains in the smaller cellulose particles as well as by a hydrolysis mechanism based on surface erosion of the microfibril bundles. The relatively large dimensions of the particles seen in the AFM images (Figure 1a in paper **V**) indicated that the individual whiskers consisted of small bundles of microfibrils rather than single crystals, as somewhat misleadingly suggested by the term cellulose nanocrystals (CNC) used for many kinds of rod-like particles in the literature (Moon et al., 2011). The limited crystal length of around 20 nm (Table 1), determined from the 004 reflection of cellulose Iβ, also demonstrated that the whiskers consisted of several crystals in their longitudinal direction. In any case, the observed characteristics of the whiskers resembled those reported by others (Elazzouzi-Hafraoui et al., 2008). Besides describing some of the fundamental properties of a type of cellulose whiskers, paper **V** also provided information that can be utilized in the preparation of for instance composite materials. In order to benefit from the nanodimensions of the cellulose whiskers in these applications, extensive irreversible aggregation of the components during drying should be prevented. Thus, the results of paper **V** suggest that the most feasible drying technique would be the uninterrupted freeze-drying. However, even more promising results for industrial applications have been reached with spray-drying (Peng et al., 2012).

3.4 General remarks

As discussed in Section 1.3.1, the determination of cellulose crystallinity is seldom a straightforward task. This is due to several reasons, among which are the varying definitions for the crystalline and amorphous fractions of cellulose, method-specific challenges in extracting the value for crystallinity from the data, and the overall complex architecture and composition of lignocellulosic biomass. Despite of these challenges, the results obtained for crystallinity in the works included in this thesis seem reasonable and fairly consistent with each other (Table 1). A value of 24% was obtained for the sample crystallinity of native birch, which was estimated to correspond to a cellulose crystallinity of about 60% (Table 1, paper **I**). When subjected to pressurized hot water treatment, the sample crystallinity increased to 30% by the removal of amorphous hemicelluloses and lignin. The cellulose crystallinity in the extracted sawdust corresponded to about 45%, which can be regarded as a typical value for cellulose-rich materials: according to Table 1, the crystallinity of cellulose in MCC, NFC, and cellulose whiskers was in the range from 48 to 58%. This range also includes the enzymatically hydrolysed

MCC as well as some of the residues remaining after the enzymatic hydrolysis of NFC with reduced xylan content. On the other hand, it was shown in paper **V** that the crystallinity values determined for the whiskers and their raw material MCCs with solid-state NMR (58–63%) were close to those obtained with WAXS. To summarize, the results indicate that in a cellulosic material with preserved fibrillar structure, a considerable proportion of the cellulose is in less ordered state. Based on the convergence between the crystallinities determined with WAXS and NMR, as well as the preservation of the crystallinity in a wide range of treatments throughout this thesis, it seems plausible that most of the non-crystalline cellulose would correspond to the cellulose chains located on the microfibril and crystal surfaces. Possible reasons for the necessity of disorder on the surface can be found in the structure and morphology of the microfibril bundles, in which the adjacent crystals could be differently oriented around their common longitudinal axis and separated by a partly hydrated layer of hemicelluloses (as illustrated in Figure 5 and discussed in Section 1.2.3).

The dimensions of cellulose crystals were calculated from WAXS data using the Scherrer equation (Equation 8), resulting in crystal widths varying from 3.2 nm for native birch wood to 4.0–5.5 nm for variously processed celluloses (Table 1). As already mentioned, the main faults of this method are the difficult choice of the line shape used for fitting and the fact that the calculation does not take into account any distribution in the crystal size (Fink et al., 1995; Jakob et al., 1995). The emphasizing effect of larger crystals was used to explain some of the results obtained in this thesis, especially when smaller lateral dimensions of the microfibrils were suggested by SAXS, as in paper **I**. The problem of SAXS, on the other hand, is that reliable determination of fibril dimensions requires the use of a model to be fitted to the experimental data. In the papers included in this work, no such specific model was assumed or fitted, but the SAXS and SANS data were quantified on the basis of peak or shoulder locations, power laws and the empirical function of paper **IV**. For these reasons, a comprehensive comparison of the crystal and fibril dimensions obtained with WAXS and SAXS was not possible. However, the results of the papers indicate that the location of the shoulder feature observed in almost all cellulosic samples containing fibrillar aggregates can be related to the lateral microfibril diameter in samples with closely associated microfibrils. The obtained distance also roughly corresponded to the lateral crystal size determined with WAXS. In the NFC samples studied in paper **IV**, the shoulder feature observed in the small-angle scattering curves could also be related to the distance between adjacent microfibrils, even though the microfibrils were not expected to be in close contact with each other.

One of the quantities determined with SAXS was the specific surface area, for which the Porod law behaviour of the scattering intensity on large q values was evaluated (based on Equation 11). The values obtained for the different cellulosic materials varied significantly, which was to be expected taking into account that the surface

area per volume reached by water is of different order of magnitude than that of the larger air-filled pores or particle surfaces (Kocherbitov et al., 2008). In this light, the values presented in Table 2 are in good agreement with results from other methods like N_2 adsorption (Kocherbitov et al., 2008; Lu and Hsieh, 2010; Zhang and Lynd, 2004). They are also consistent with each other, showing for instance smaller values for freeze-dried native birch than for dry MCC powders. For the wet enzymatically hydrolysed MCCs, the specific surface areas were almost two orders of magnitude higher, which is readily explained by the penetration of water to the spaces between individual microfibrils. Thus, the results confined in this thesis demonstrate the potential of SAXS in determining specific surface areas of cellulosic materials well comparable with other methods.

4 Conclusions and future aspects

An understanding on the fundamental structure of native cellulosic biomasses is highly beneficial, if not essential, for their efficient utilization in the context of biorefining. However, despite of the enormous research efforts made in the area over the years, our knowledge on these materials is still relatively restricted. It may well be that because of the complexity and diversity of biological systems, a comprehensive understanding on their structure and interactions will remain a long-lasting challenge. Nevertheless, even modest extensions to our knowledge can help to improve the current processes utilizing biomass and lead to the development of new applications in the field of biomass refining and elsewhere. Even though most of the steps on this path are able to elucidate only minor pieces of the whole puzzle, which in the particular case of biomaterials is far from a simple one, each of the individual steps has their significance and role as part of the larger picture.

The main observations reported in papers **I**–**V** can be summarized in the following:

- Pressurized hot water extraction of birch sawdust increased the width of cellulose crystallites and led to denser packing of individual cellulose microfibrils, whereby larger pores were opened in between the microfibril bundles.

- The enzymatic hydrolysis of MCC was limited by the aggregation of cellulose microfibrils, which caused the preservation of the average nanoscale structural properties, such as crystallinity, even though changes in larger structures could be observed.

- The enzymatic degradation of NFC, regarding both the cellulose crystallites and the fibrillar network structure, was enhanced by a specific hydrolysis of xylan prior to the fibrillation, whereas the remaining fraction of xylan stayed in close contact with cellulose without largely resisting the hydrolysis.

- Preparation of cellulose whiskers from MCC did not affect their crystallinity or crystal size, whereas differences in the nanoscale packing and thermal properties of dried whiskers were observed as a function of drying method, surface charge neutralization, and the source of MCC.

When considering the results of this thesis in a broader context, one of the topics to be highlighted is that of the behaviour of cellulose crystallinity in the various treatments, including its preservation in the enzymatic hydrolysis of MCC (paper **II**) and during the preparation of cellulose whiskers (paper **V**). The observed behaviour can be seen to complement the picture outlined for the structure of fibrillar celluloses in Section 1.2.3, even though many unanswered questions still remain. In fact, the crystallinity represents one of the fundamental properties of cellulose that is still not

understood well enough to predict its behaviour or role under different circumstances. As it seems that the widest gaps in our current knowledge are related to the characteristics of the more and less ordered supramolecular structures of cellulose and their roles in the various chemical and physical reactions, the investigation in this area should be promoted. This could be done in particular by applying complementary experimental methods and by utilizing the obtained information in collaboration among specialists of different fields. Besides purely experimental methods, computer simulations on cellulose crystals and modelling of diffraction patterns can also make an important contribution to this topic.

The fibrillar structure of cellulose is also a subject requiring more investigation. One of the merits of this thesis is that it, once again, brought forward the applicability of small-angle x-ray and neutron scattering methods in shedding light to various research problems related to the nanoscale structure of cellulose. Even though a complete identification of the different features observed in small-angle scattering intensities of fibrillar celluloses is not yet possible, some of them, such as the shoulder feature discussed in Sections 1.3 and 3, can already be linked to relatively well-defined structures. To proceed from this, the use of neutron scattering and contrast variation opens great opportunities to further deepen our understanding on the fibrillar structure of cellulose. The possibilities of neutron scattering were demonstrated by the deuterium labelling used by Nishiyama et al. (2003) to emphasize the amorphous regions in cellulose microfibrils, which led to the discovery of their periodical arrangement in ramie fibres. Systematic studies of the same kind should be continued together with for instance high-resolution AFM techniques, which have shown considerable potential in the field (Bubner et al., 2013). By applying several methods together, the mysteries related to the amorphous regions and also to the longitudinal structure of cellulose microfibrils could likely be unravelled.

A practical point for development related to the small-angle scattering techniques used in this thesis could be found in the application of the specific surface determination based on the Porod law. This method could be upgraded by improvements related to the determination of volume fractions especially in wet samples and by correlating its results to the other available techniques by standardized biomass-based materials. As compared to N_2 adsorption and some of the other methods used for the determination of specific surface, SAXS benefits especially from the possibility to carry out measurements under both dry and wet conditions and without complicated sample preparation procedures. Therefore, more efforts should be made to develop it further in the context of cellulosic materials.

Among the specific research problems discussed by the works included in this thesis, the main focus was on the enzymatic hydrolysis of cellulose and in particular on its structural limiting factors. The important role of the structural properties of the substrate material for the efficiency and mechanism of the hydrolysis, as well as the

evolution of the structures during the treatment could be demonstrated. As the inefficiency of the enzymatic hydrolysis still restricts the full utilization wood-based biomass for the production of liquid biofuels and chemicals, systematic studies with well-defined substrates and competent characterization methods should be continued to elucidate the factors responsible for the slowing down of the hydrolysis. The alternative route of developing better enzymes using the tools of biotechnology should also be supported by investigating the effects of the novel enzymes on the lignocellulose structure as thoroughly as has been done for the conventional ones. Again, collaboration and dialogue between scientists from different fields will be essential to reach a comprehensive understanding on the complicated topics. As the biomaterials themselves do not adhere to a simple division between different disciplines and to other human-based categorization, this kind of multidisciplinary approach, adopted throughout this thesis, will probably prove fruitful in a number of research cases related to the field of natural sciences.

References

Åkerholm, M. and Salmén, L. (2001). Interactions between wood polymers studied by dynamic FT-IR spectroscopy. *Polymer*, 42:963–969.

Als-Nielsen, J. and McMorrow, D. (2001). *Elements of Modern X-Ray Physics*. John Wiley & Sons.

Alvira, P., Tomás-Pejó, E., Ballesteros, M., and Negro, M. J. (2010). Pretreatment technologies for an efficient bioethanol production process based on enzymatic hydrolysis: a review. *Bioresour. Technol.*, 101:4851–4861.

Andersson, S., Serimaa, R., Paakkari, T., Saranpää, P., and Pesonen, E. (2003). Crystallinity of wood and the size of cellulose crystallites in Norway spruce (*Picea abies*). *J. Wood Sci.*, 49:531–537.

Arantes, V. and Saddler, J. N. (2010). Access to cellulose limits the efficiency of enzymatic hydrolysis: the role of amorphogenesis. *Biotechnol. Biofuels*, 3:4.

Arola, S., Malho, J.-M., Laaksonen, P., Lille, M., and Linder, M. B. (2013). The role of hemicellulose in nanofibrillated cellulose networks. *Soft Matter*, 9:1319–1326.

Astley, O. M. and Donald, A. M. (2001). A small-angle x-ray scattering study of the effect of hydration on the microstructure of flax fibers. *Biomacromolecules*, 2:672–680.

Atalla, R. H. and VanderHart, D. L. (1984). Native cellulose: a composite of two distinct crystalline forms. *Science*, 223:283–285.

Atkins, P. and de Paula, J. (2010). *Atkins' Physical Chemistry*. Oxford University Press, 9th edition.

Awano, T., Takabe, K., and Fujita, M. (2002). Xylan deposition on secondary wall of *Fagus crenata* fiber. *Protoplasma*, 219:106–115.

Azizi Samir, M. A. S., Alloin, F., and Dufresne, A. (2005). Review of recent research into cellulosic whiskers, their properties and their application in nanocomposite field. *Biomacromolecules*, 6:616–626.

Bacon, G. E. (1977). *Neutron Scattering in Chemistry*. Butterworths.

Bansal, P., Hall, M., Realff, M. J., Lee, J. H., and Bommarius, A. S. (2010). Multivariate statistical analysis of X-ray data from cellulose: a new method to determine degree of crystallinity and predict hydrolysis rates. *Bioresour. Technol.*, 101:4461–4471.

Bansal, P., Vowell, B. J., Hall, M., Realff, M. J., Lee, J. H., and Bommarius, A. S. (2012). Elucidation of cellulose accessibility, hydrolysability and reactivity as the major limitations in the enzymatic hydrolysis of cellulose. *Bioresour. Technol.*, 107:243–250.

Battista, O. A. (1950). Hydrolysis and crystallization of cellulose. *Ind. Eng. Chem.*, 42:502–507.

Brown Jr., R. M. and Saxena, I. M. (2000). Cellulose biosynthesis: a model for understanding the assembly of biopolymers. *Plant Physiol. Biochem.*, 38:57–67.

Bubner, P., Plank, H., and Nidetzky, B. (2013). Visualizing cellulase activity. *Biotechnol. Bioeng.*, 110:1529–1549.

Cateto, C., Hu, G., and Ragauskas, A. (2011). Enzymatic hydrolysis of organosolv Kanlow switchgrass and its impact on cellulose crystallinity and degree of polymerization. *Energy Environ. Sci.*, 4:1516–1521.

Chanzy, H. (2011). The continuing debate over the structure of cellulose: historical perspective and outlook. *Cellulose*, 18:853–856.

Cheng, G., Varanasi, P., Li, C., Liu, H., Melnichenko, Y. B., Simmons, B. A., Kent, M. S., and Singh, S. (2011). Transition of cellulose crystalline structure and surface morphology of biomass as a function of ionic liquid pretreatment and its relation to enzymatic hydrolysis. *Biomacromolecules*, 12:933–941.

Chundawat, S. P. S., Beckham, G. T., Himmel, M. E., and Dale, B. E. (2011). Deconstruction of lignocellulosic biomass to fuels and chemicals. *Annu. Rev. Chem. Biomol. Eng.*, 2:121–145.

Chunilall, V., Bush, T., Larsson, P. T., Iversen, T., and Kindness, A. (2010). A CP/MAS ^{13}C-NMR study of cellulose fibril aggregation in eucalyptus dissolving pulps during drying and the correlation between aggregate dimensions and chemical reactivity. *Holzforschung*, 64:693–698.

Cosgrove, D. J. (2005). Growth of the plant cell wall. *Nat. Rev. Mol. Cell Biol.*, 6:850–861.

Cullity, B. D. and Stock, S. R. (2001). *Elements of X-Ray Diffraction*. Prentice Hall, 3rd edition.

Donaldson, L. (2007). Cellulose microfibril aggregates and their size variation with cell wall type. *Wood Sci. Technol.*, 41:443–460.

Dong, X. M., Revol, J.-F., and Gray, D. G. (1998). Effect of microcrystallite preparation conditions on the formation of colloid crystals of cellulose. *Cellulose*, 5:19–32.

Driemeier, C. and Bragatto, J. (2013). Crystallite width determines monolayer hydration across a wide spectrum of celluloses isolated from plants. *J. Phys. Chem. B*, 117:415–421.

Driemeier, C. and Calligaris, G. A. (2011). Theoretical and experimental developments for accurate determination of crystallinity of cellulose I materials. *J. Appl. Crystallogr.*, 44:184–192.

Driemeier, C., Pimenta, M. T. B., Rocha, G. J. M., Oliveira, M. M., Mello, D. B., Maziero, P., and Gonçalves, A. R. (2011). Evolution of cellulose crystals during prehydrolysis and soda delignification of sugarcane lignocellulose. *Cellulose*, 18:1509–1519.

Eichhorn, S. J. (2011). Cellulose nanowhiskers: promising materials for advanced applications. *Soft Matter*, 7:303–315.

Elazzouzi-Hafraoui, S., Nishiyama, Y., Putaux, J.-L., Heux, L., Dubreuil, F., and Rochas, C. (2008). The shape and size distribution of crystalline nanoparticles prepared by acid hydrolysis of native cellulose. *Biomacromolecules*, 9:57–65.

Evans, R., Newman, R. H., Roick, U. C., Suckling, I. D., and Wallis, A. F. A. (2005). Changes in cellulose crystallinity during kraft pulping. Comparison of infrared, x-ray diffraction and solid state NMR results. *Holzforschung*, 12:498–504.

Fahlén, J. and Salmén, L. (2003). Cross-sectional structure of the secondary wall of wood fibers as affected by processing. *J. Mater. Sci.*, 38:119–126.

Fahlén, J. and Salmén, L. (2005). Pore and matrix distribution in the fiber wall revealed by atomic force microscopy and image analysis. *Biomacromolecules*, 6:433–438.

Faruk, O., Bledzki, A. K., Fink, H.-P., and Sain, M. (2012). Biocomposites reinforced with natural fibers: 2000–2010. *Prog. Polym. Sci.*, 37:1552–1596.

Feigin, L. A. and Svergun, D. I. (1987). *Structure Analysis by Small-Angle X-Ray and Neutron Scattering*. Plenum Press.

Fernandes, A. N., Thomas, L. H., Altaner, C. M., Callow, P., Forsyth, V. T., Apperley, D. C., Kennedy, C. J., and Jarvis, M. C. (2011). Nanostructure of cellulose microfibrils in spruce wood. *Proc. Natl. Acad. Sci. U.S.A.*, 108:E1195–E1203.

Fink, H.-P., Hofmann, D., and Philipp, B. (1995). Some aspects of lateral chain order in cellulosics from X-ray scattering. *Cellulose*, 2:51–70.

Fink, H.-P., Hofmann, D., and Purz, H. J. (1990). On the fibrillar structure of native cellulose. *Acta Polymerica*, 41:131–137.

Fink, H.-P., Philipp, B., Zschunke, C., and Hayn, M. (1992). Structural changes of LODP cellulose in the original and mercerized state during enzymatic hydrolysis. *Acta Polymerica*, 43:270–274.

Frey-Wyssling, A. (1954). The fine structure of cellulose microfibrils. *Science*, 119:80–82.

Ganner, T., Bubner, P., Eibinger, M., Mayrhofer, C., Plank, H., and Nidetzky, B. (2012). Dissecting and reconstructing synergism – in situ visualization of cooperativity among cellulases. *J. Biol. Chem.*, 287:43215–43222.

Gedde, U. W. (1995). *Polymer Physics*. Springer.

Gomez, L. D., Steele-King, C. G., and McQueen-Mason, S. J. (2008). Sustainable liquid biofuels from biomass: the writings on the walls. *New Phytologist*, 178:473–485.

Graham-Rowe, D. (2011). Agriculture: beyond food versus fuel. *Nature*, 474:S6–S8.

Gross, A. S. and Chu, J.-W. (2010). On the molecular origins of biomass recalcitrance: the interaction network and solvation structures of cellulose microfibrils. *J. Phys. Chem. B*, 114:13333–13341.

Guerriero, G., Fugelstad, J., and Bulone, V. (2010). What do we really know about cellulose biosynthesis in higher plants? *J. Integr. Plant Biol.*, 52:161–175.

Hanley, S. J., Revol, J.-F., Godbout, L., and Gray, D. G. (1997). Atomic force microscopy and transmission electron microscopy of cellulose from *Micrasterias denticulata*; evidence for a chiral helical microfibril twist. *Cellulose*, 4:209–220.

Herrick, F. W., Casebier, R. L., Hamilton, J. K., and Sandberg, K. R. (1983). Microfibrillated cellulose: morphology and accessibility. *J. Appl. Polym. Sci.: Appl. Polym. Symp.*, 37:797–813.

Himmel, M. E., Ding, S.-Y., Johnson, D. K., Adney, W. S., Nimlos, M. R., Brady, J. W., and Foust, T. D. (2007). Biomass recalcitrance: engineering plants and enzymes for biofuels production. *Science*, 315:804–807.

Hosemann, R. and Bagchi, S. N. (1962). *Direct Analysis of Diffraction by Matter*. North-Holland.

Hsieh, J. (2009). *Computed Tomography: Principles, Design, Artifacts, and Recent Advances*. SPIE/Wiley Interscience, 2nd edition.

Hu, F. and Ragauskas, A. (2012). Pretreatment and lignocellulosic chemistry. *Bioenerg. Res.*, 5:1043–1066.

Ioelovich, M., Leykin, A., and Figovsky, O. (2010). Study of cellulose paracrystallinity. *BioResources*, 5:1393–1407.

Jakob, H. F., Fengel, D., Tschegg, S. E., and Fratzl, P. (1995). The elementary cellulose fibril in *Picea abies*: comparison of transmission electron microscopy, small-angle x-ray scattering, and wide-angle x-ray scattering results. *Macromolecules*, 28:8782–8787.

Jalak, J., Kurašin, M., Teugjas, H., and Väljamäe, P. (2012). Endo-exo synergism in cellulose hydrolysis revisited. *J. Biol. Chem.*, 287:28802–28815.

Jørgensen, H., Kristensen, J. B., and Felby, C. (2007). Enzymatic conversion of lignocellulose into fermentable sugars: challenges and opportunities. *Biofuels Bioprod. Biorefin.*, 1:119–134.

Kennedy, C. J., Cameron, G. J., Šturcová, A., Apperley, D. C., Altaner, C., Wess, T. J., and Jarvis, M. C. (2007). Microfibril diameter in celery collenchyma cellulose: X-ray scattering and NMR evidence. *Cellulose*, 14:235–246.

Kilpeläinen, I., Xie, H., King, A., Granstrom, M., Heikkinen, S., and Argyropoulos, D. S. (2007). Dissolution of wood in ionic liquids. *J. Agric. Food Chem.*, 55:9142–9148.

Kim, N.-H., Imai, T., Wada, M., and Sugiyama, J. (2006). Molecular directionality in cellulose polymorphs. *Biomacromolecules*, 7:274–280.

Kleman-Leyer, K. M., Siika-aho, M., Teeri, T. T., and Kirk, T. K. (1996). The cellulases endoglucanase I and cellobiohydrolase II of *Trichoderma reesei* act synergistically to solubilize native cotton cellulose but not to decrease its molecular size. *Appl. Environ. Microbiol.*, 62:2883–2887.

Klemm, D., Heublein, B., Fink, H.-P., and Bohn, A. (2005). Cellulose: fascinating biopolymer and sustainable raw material. *Angew. Chem. Int. Ed.*, 44:3358–3393.

Klug, H. P. and Alexander, L. E. (1974). *X-Ray Diffraction Procedures for Polycrystalline and Amorphous Materials.* John Wiley & Sons, 2nd edition.

Kocherbitov, V., Ulvenlund, S., Kober, M., Jarring, K., and Arnebrant, T. (2008). Hydration of microcrystalline cellulose and milled cellulose studied by sorption calorimetry. *J. Phys. Chem. B*, 112:3728–3734.

Kondo, T., Togawa, E., and Brown Jr., R. M. (2001). "Nematic ordered cellulose": a concept of glucan chain association. *Biomacromolecules*, 2:1324–1330.

Kontturi, E., Suchy, M., Penttilä, P., Jean, B., Pirkkalainen, K., Torkkeli, M., and Serimaa, R. (2011). Amorphous characteristics of an ultrathin cellulose film. *Biomacromolecules*, 12:770–777.

Langan, P., Nishiyama, Y., and Chanzy, H. (2001). X-ray structure of mercerized cellulose II at 1 Å resolution. *Biomacromolecules*, 2:410–416.

Larsson, P. T., Svensson, A., and Wågberg, L. (2013). A new, robust method for measuring average fibre wall pore sizes in cellulose I rich plant fibre walls. *Cellulose*, 20:623–631.

Leppänen, K., Andersson, S., Torkkeli, M., Knaapila, M., Kotelnikova, N., and Serimaa, R. (2009). Structure of cellulose and microcrystalline cellulose from various wood species, cotton and flax studied by X-ray scattering. *Cellulose*, 16:999–1015.

Lichtenegger, H., Müller, M., Paris, O., Riekel, C., and Fratzl, P. (1999). Imaging of the helical arrangement of cellulose fibrils in wood by synchrotron X-ray microdiffraction. *J. Appl. Crystallogr.*, 32:1127–1133.

Lindner, P. (2002). Scattering experiments: experimental aspects, initial data reduction and absolute calibration. In Lindner, P. and Zemb, T., editors, *Neutrons, X-Rays and Light: Scattering Methods Applied to Soft Condensed Matter*, pages 23–48. Elsevier.

Lu, P. and Hsieh, Y.-L. (2010). Preparation and properties of cellulose nanocrystals: Rods, spheres,and network. *Carbohydr. Polym.*, 82:329–336.

Mansfield, S. D., Mooney, C., and Saddler, J. N. (1999). Substrate and enzyme characteristics that limit cellulose hydrolysis. *Biotechnol. Prog.*, 15:804–816.

Matthews, J. F., Himmel, M. E., and Crowley, M. F. (2012). Conversion of cellulose Iα to Iβ via a high temperature intermediate (I-HT) and other cellulose phase transformations. *Cellulose*, 19:297–306.

Matthews, J. F., Skopec, C. E., Mason, P. E., Zuccato, P., Torget, R. W., Sugiyama, J., Himmel, M. E., and Brady, J. W. (2006). Computer simulation studies of microcrystalline cellulose Iβ. *Carbohydr. Res.*, 341:138–352.

Moon, R. J., Martini, A., Nairn, J., Simonsen, J., and Youngblood, J. (2011). Cellulose nanomaterials review: structure, properties and nanocomposites. *Chem. Soc. Rev.*, 40:3941–3994.

Mosier, N., Wyman, C., Dale, B., Elander, R., Lee, Y. Y., Holtzapple, M., and Ladisch, M. (2005). Features of promising technologies for pretreatment of lignocellulosic biomass. *Bioresour. Technol.*, 96:673–686.

Newman, R. H. (1999). Estimation of the lateral dimensions of cellulose crystallites using ^{13}C NMR signal strengths. *Solid State Nucl. Magn. Reson.*, 15:21–29.

Nishikawa, S. and Ono, S. (1913). Transmission of x-rays through fibrous, lamellar and granular substances. *Proc. Tokyo Math. Phys. Soc*, 7:131–138.

Nishiyama, Y. (2009). Structure and properties of the cellulose microfibril. *J. Wood. Sci.*, 55:241–249.

Nishiyama, Y., Johnson, G. P., and French, A. D. (2012). Diffraction from nonperiodic models of cellulose crystals. *Cellulose*, 19:319–336.

Nishiyama, Y., Kim, U.-J., Kim, D.-Y., Katsumata, K. S., May, R. P., and Langan, P. (2003). Periodic disorder along ramie cellulose microfibrils. *Biomacromolecules*, 4:1013–1017.

Nishiyama, Y., Langan, P., and Chanzy, H. (2002). Crystal structure and hydrogen-bonding system in cellulose Iβ from synchrotron x-ray and neutron fiber diffraction. *J. Am. Chem. Soc.*, 124:9074–9082.

Olsson, A.-M., Bjurhager, I., Gerber, L., Sundberg, B., and Salmén, L. (2011). Ultrastructural organisation of cell wall polymers in normal and tension wood of aspen revealed by polarisation FTIR microspectroscopy. *Planta*, 233:1277–1286.

O'Sullivan, A. C. (1997). Cellulose: the structure slowly unravels. *Cellulose*, 4:173–207.

Paakkari, T., Serimaa, R., and Fink, H.-P. (1989). Structure of amorphous cellulose. *Acta Polymerica*, 40:731–734.

Pääkkö, M., Ankerfors, M., Kosonen, H., Nykänen, A., Ahola, S., Österberg, M., Ruokolainen, J., Laine, J., Larsson, P. T., Ikkala, O., and Lindström, T. (2007). Enzymatic hydrolysis combined with mechanical shearing and high-pressure homogenization for nanoscale cellulose fibrils and strong gels. *Biomacromolecules*, 8:1934–1941.

Paavilainen, S., Róg, T., and Vattulainen, I. (2011). Analysis of twisting of cellulose nanofibrils in atomistic molecular dynamics simulations. *J. Phys. Chem. B*, 115:3747–3755.

Park, S., Baker, J. O., Himmel, M. E., Parilla, P. A., and Johnson, D. K. (2010). Cellulose crystallinity index: measurement techniques and their impact on interpreting cellulase performance. *Biotechnol. Biofuels*, 3:10.

Pedersen, M. and Meyer, A. S. (2010). Lignocellulose pretreatment severity – relating pH to biomatrix opening. *New Biotechnol.*, 27:739–750.

Peng, Y., Gardner, D. J., and Han, Y. (2012). Drying cellulose nanofibrils: in search of a suitable method. *Cellulose*, 19:91–102.

Pönni, R., Vuorinen, T., and Kontturi, E. (2012). Proposed nano-scale coalescence of cellulose in chemical pulp fibers during technical treatments. *BioResources*, 7:6077–6108.

Porod, G. (1982). General theory. In Glatter, O. and Kratky, O., editors, *Small Angle X-ray Scattering*, pages 17–51. Academic Press.

Ragauskas, A. J., Williams, C. K., Davison, B. H., Britovsek, G., Cairney, J., Eckert, C. A., Frederick Jr., W. J., Hallett, J. P., Leak, D. J., Liotta, C. L., Mielenz, J. R., Murphy, R., Templer, R., and Tschaplinski, T. (2006). The path forward for biofuels and biomaterials. *Science*, 311:484–489.

Rånby, B. G. (1951). Fibrous macromolecular systems. Cellulose and muscle. The colloidal properties of cellulose micelles. *Discuss. Faraday Soc.*, 11:158–164.

Ruel, K., Nishiyama, Y., and Joseleau, J.-P. (2012). Crystalline and amorphous cellulose in the secondary walls of Arabidopsis. *Plant Sci.*, 193–194:48–61.

Ruland, W. (1961). X-ray determination of crystallinity and diffuse disorder scattering. *Acta Crystallogr.*, 14:1180–1185.

Salmén, L., Olsson, A.-M., Stevanic, J. S., Simonović, J., and Radotić, K. (2012). Structural organisation of the wood polymers in the wood fibre structure. *BioResources*, 7:521–532.

Samayam, I. P., Hanson, B. L., Langan, P., and Schall, C. A. (2011). Ionic-liquid induced changes in cellulose structure associated with enhanced biomass hydrolysis. *Biomacromolecules*, 12:3091–3098.

Schenzel, K., Fischer, S., and Brendler, E. (2005). New method for determining the degree of cellulose I crystallinity by means of FT Raman spectroscopy. *Cellulose*, 12:223–231.

Schmidt, P. W. (1991). Small-angle scattering studies of disordered, porous and fractal systems. *J. Appl. Crystallogr.*, 24:414–435.

Schultz, T. P. and Taylor, F. E. (1989). Wood. In Kitani, O. and Hall, C. W., editors, *Biomass Handbook*. Gordon and Breach Science Publishers.

Segal, L., Creely, J. J., Martin Jr., A. E., and Conrad, C. M. (1959). Degree of crystallinity of native cellulose using the x-ray diffractometer. *Text Res. J.*, 29:786–794.

Siró, I. and Plackett, D. (2010). Microfibrillated cellulose and new nanocomposite materials: a review. *Cellulose*, 17:459–494.

Sjöström, E. (1993). *Wood Chemistry: Fundamentals and Application*. Academic Press, 2nd edition.

Spalla, O., Lyonnard, S., and Testard, F. (2003). Analysis of the small-angle intensity scattered by a porous and granular medium. *J. Appl. Crystallogr.*, 36:338–347.

Stevanic, J. S. and Salmén, L. (2009). Orientation of the wood polymers in the cell wall of spruce wood fibres. *Holzforschung*, 63:497–503.

Teeri, T. T. (1997). Crystalline cellulose degradation: new insight into the function of cellobiohydrolases. *Tibtech*, 15:160–167.

Terashima, N., Kitano, K., Kojima, M., Yoshida, M., Yamamoto, H., and Westermark, U. (2009). Nanostructural assembly of cellulose, hemicellulose, and lignin in the middle layer of secondary wall of ginkgo tracheid. *J. Wood Sci.*, 55:409–416.

Thygesen, A., Oddershede, J., Lilholt, H., Thomsen, A. B., and Ståhl, K. (2005). On the determination of crystallinity and cellulose content in plant fibres. *Cellulose*, 12:563–576.

Tolonen, L. K., Zuckerstätter, G., Penttilä, P. A., Milacher, W., Habicht, W., Serimaa, R., Kruse, A., and Sixta, H. (2011). Structural changes in microcrystalline cellulose in subcritical water treatment. *Biomacromolecules*, 12:2544–2551.

Turbak, A. F., Snyder, F. W., and Sandberg, K. R. (1983). Microfibrillated cellulose, a new cellulose product: properties, uses, and commercial potential. *J. Appl. Polym. Sci.: Appl. Polym. Symp.*, 37:815–827.

Viikari, L., Vehmaanperä, J., and Koivula, A. (2012). Lignocellulosic ethanol: from science to industry. *Biomass Bioenergy*, 46:13–24.

Vonk, C. G. (1973). Computerization of Ruland's X-ray method for determination of the crystallinity in polymers. *J. Appl. Crystallogr.*, 6:148–152.

Wickholm, K., Larsson, P. T., and Iversen, T. (1998). Assignment of non-crystalline forms in cellulose I by CP/MAS ^{13}C NMR spectroscopy. *Carbohydr. Res.*, 312:123–129.

Zhang, Y.-H. P. and Lynd, L. R. (2004). Toward an aggregated understanding of enzymatic hydrolysis of cellulose: Noncomplexed cellulase systems. *Biotechnol. Bioeng.*, 88:797–824.

Zugenmaier, P. (2001). Conformation and packing of various crystalline cellulose fibers. *Prog. Polym. Sci.*, 26:1341–1417.